



RESEARCH ARTICLE

Published in tribute to the life and scientific achievements of Dr. John F. Fallon.
Article invited by Dr. Matt Harris, Harvard Medical School.

Dbx2 regulation in limbs suggests interTAD sharing of enhancers

Leonardo Beccari^{1,2}  | Gabriel Jaquier¹ | Lucille Lopez-Delisle³ |
Eddie Rodriguez-Carballo^{1,4} | Bénédicte Mascrez¹ | Sandra Gitto¹ |
Joost Woltering^{1,5} | Denis Duboule^{1,3,6} 

¹Department of Genetics and Evolution, University of Geneva, Geneva, Switzerland

²Institut NeuroMyoGène, CNRS UMR 5310, INSERM U1217, University Claude Bernard Lyon1, Lyon, France

³School of Life Sciences, Federal School of Technology (EPFL), Lausanne, Switzerland

⁴Department of Molecular Biology, University of Geneva, Geneva, Switzerland

⁵Zoology and Evolutionary Biology, Department of Biology, University of Konstanz, Konstanz, Germany

⁶Collège de France, Paris, France

Correspondence

Leonardo Beccari and Denis Duboule, Department of Genetics and Evolution, University of Geneva, Geneva, Switzerland. Email: leonardo.beccari@univ-lyon1.fr (L. B.) and denis.duboule@unige.ch; denis.duboule@epfl.ch (D. D.)

Funding information

H2020 European Research Council, Grant/Award Number: 588029; Schweizerischer Nationalfonds zur Förderung der Wissenschaftlichen Forschung, Grant/Award Number: 310030B_138662

Abstract

Background: During tetrapod limb development, the HOXA13 and HOXD13 transcription factors are critical for the emergence and organization of the autopod, the most distal aspect where digits will develop. Since previous work had suggested that the *Dbx2* gene is a target of these factors, we set up to analyze in detail this potential regulatory interaction.

Results: We show that HOX13 proteins bind to mammalian-specific sequences at the vicinity of the *Dbx2* locus that have enhancer activity in developing digits. However, the functional inactivation of the DBX2 protein did not elicit any particular phenotype related to *Hox* genes inactivation in digits, suggesting either redundant or compensatory mechanisms. We report that the neighboring *Nell2* and *Ano6* genes are also expressed in distal limb buds and are in part controlled by the same *Dbx2* enhancers despite being localized into two different topologically associating domains (TADs) flanking the *Dbx2* locus.

Conclusions: We conclude that *Hoxa13* and *Hoxd* genes cooperatively activate *Dbx2* expression in developing digits through binding to mammalian specific regulatory sequences in the *Dbx2* neighborhood. Furthermore, these enhancers can overcome TAD boundaries in either direction to co-regulate a set of genes located in distinct chromatin domains.

KEYWORDS

chromatin architecture, digit development, gene regulation, *Hox*, TAD boundary

1 | INTRODUCTION

For many decades, the vertebrate limb has been an efficient experimental paradigm to study the basic principles

and concepts underlying developmental processes. The main reason is the congruence between the definition of specific signaling regions in the developing limb buds, on the one hand, and their association with specific

This is an open access article under the terms of the Creative Commons Attribution-NonCommercial-NoDerivs License, which permits use and distribution in any medium, provided the original work is properly cited, the use is non-commercial and no modifications or adaptations are made.

© 2021 The Authors. *Developmental Dynamics* published by Wiley Periodicals LLC on behalf of American Association of Anatomists.

molecular markers, on the other hand. Classical experimental embryology indeed led to a fairly precise cellular definition of those regions in the limb bud, which have a particular activity and function, such as the limb apical ectodermal ridge and the zone of polarizing activity.^{1,2} John Fallon made seminal contributions in this early phase and was one of the pioneers of this field;³ see also in References 4, 5, as well as.^{6,7,8,9} Subsequently, transcription factors were cloned, which could be superimposed to such cellular landmarks, such as *Hox* genes¹⁰ (see Reference 11), followed by the key signaling molecules.¹²⁻¹⁴ Soon after, gain- and loss-of-function experiments helped ascertain the central roles of these genes in controlling limb patterning and morphogenesis. In this view, the developing limb was the first vertebrate system where a solid bridge was established between cellular models and their molecular components.

Among these key factors are the *Hox* genes belonging to both the *HoxA* and *HoxD* clusters. They are transcribed into precisely delimited domains within the incipient limb buds^{8,13} and they specify the proximal and distal limb segments as well as some anterior to posterior features¹⁶⁻¹⁸ (reviewed in Reference 19). *Hoxa13* and *Hoxd13* are essentially required for the specification and development of the autopod, the distal-most limb domain that will give rise to the digits and part of the wrist. They control the size, shape, and number of autopod bones by regulating mesenchymal cell aggregation, chondrification, and ossification.^{17,20-22} In fact, the inactivation of both *Hoxa13* and *Hoxd13* in mice leads to an agenesis of the distal limb and the formation of a chondrogenic blastema at the distal extremity of the ulna/fibula and radius/humerus.^{17,18} Different studies have addressed the identification of the HOXA13/HOXD13 downstream target genes in distal limb development. These included genes controlling cell adhesion, morphology, and proliferation/survival (e.g., *Hand2*, *Shh*, *EphA7*, *EphA3*, and *Bmp2/Bmp7*).²³⁻²⁹ The regulatory relationships and functional roles of many such target genes nevertheless remain poorly understood.

We previously reported that the transcription factor *Dbx2* (*Developing Brain Homeobox protein 2*) is strongly down-regulated in distal forelimb cells lacking *Hox13* function.²³ *Dbx2* belongs to the *Dbx* subfamily of homeobox-containing proteins and is expressed in the mouse embryonic brain and neural tube, as well as during limb development.^{23,30,31} However, while it is well established that *Dbx2* contributes to the specification of the V0 spinal cord interneurons,³²⁻³⁵ its potential role in limb development has remained elusive. A heterozygote deletion spanning the genomic region comprising the human loci *NELL2*, *DBX2*, and *ANO6* was nevertheless associated with intellectual retardation, skeletal and dental anomalies, reduced hand and feet size and clinodactyly of the fifth digit, suggesting that *Dbx2* could

be involved in digit development,³⁶ where it may mediate part of the functions of HOX13 proteins.

In this study, we characterized the regulation of the mouse *Dbx2* gene in developing digits. We show that the HOX13 factors directly regulate *Dbx2* expression in digits, in part by binding to mammalian-specific regulatory elements located within 30 kb 5' to the *Dbx2* locus, as well as within its introns. Furthermore, we show that 5' *Hoxd* genes also contribute to *Dbx2* regulation by acting cooperatively and redundantly with HOX13 proteins. However, *Dbx2* null mice do not display any of the major limb skeletal abnormalities displayed by any combinations of HOX mutations, suggesting either that *Dbx2* is not a major downstream *Hox* effector or that its function is compensated for in this particular situation.

We also observed that the *Dbx2* neighboring genes *Nell2* (*Neural EGFL Like 2*) and *Ano6* (*Anoctamin 6*) are also expressed in the distal limb. Analysis of chromatin interaction profiles revealed that, at the 3D level, the *Nell2* and *Ano6* genes are organized into distinct topologically associating domains (TADs), which are regions of the genome where gene-enhancer interactions are favored.³⁷ Interestingly, the boundary between these two TADs maps at the proximity of the *Dbx2* locus and of its limb enhancers, which seem to be able to control the transcription of the three genes, regardless of in which TAD they reside.

2 | RESULTS

2.1 | *Dbx2* expression during distal limb development

We characterized *Dbx2* expression at different stages of mouse forelimb development by whole-mount in situ hybridization (WISH) and compared it with that of *Hoxa13* and *Hoxd13* (Figure 1). *Dbx2* transcripts were first scored during early limb development (E9.5-E10) throughout the limb bud mesenchyme, with the exception of mesodermal cells underlying the distal-most limb ectoderm (Figure 1A). This expression poorly correlates with that of *Hox13* genes (Figure 1B) and, overall, the *Dbx2* mRNA levels at this stage remained very low. By E11.5, proximal *Dbx2* expression was confined to a small and posterior moon-shaped cellular domain (Figure 1A, asterisk). *Dbx2* transcripts were also detected in the anterior portion of the autopod (Figure 1A, arrowhead). Thus, the distal limb expression of *Dbx2* was delayed by approximately 24 hours when compared to the onset of *Hoxa13* and *Hoxd13* in the autopod (Figure 1A, B).^{10,38} At E12.5, *Dbx2* mRNA spread to the entire distal-most portion of the autopod, both in digit and interdigit mesoderm and in a nested domain within the *Hoxa13/Hoxd13* expressing cells (Figure 1A,B). However, *Dbx2* transcripts were

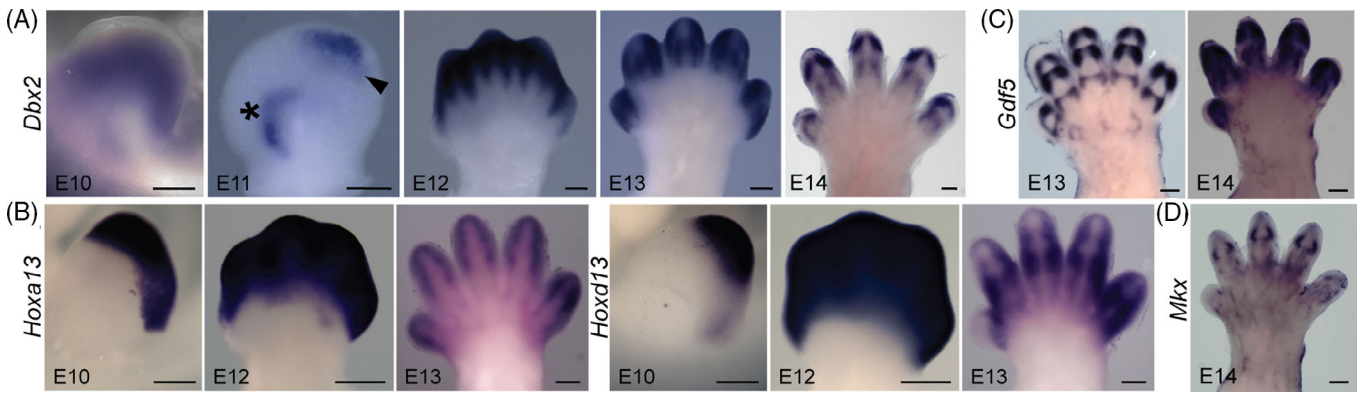


FIGURE 1 Analysis of *Dbx2* expression in developing digits. A–D, WISH analysis of *Dbx2*, A, and *Hoxa13/Hoxd13*, B, *Gdf5*, C, and *Mlx*, D, in mouse embryonic forelimbs at different developmental stages. Scale bar: 250 μ m

rapidly downregulated in the interdigit region and, from E13 onwards, they were detected in sequentially formed domains reminiscent of the digit joints (Figure 1A,C,D).

To assess which cell type(s) express the *Dbx2* gene, we re-analyzed single cell-RNA sequencing (scRNA-seq) data sets from E11, E13, and E15 mouse hindlimbs³⁹ (Figure 2). At E11.5 *Dbx2* is expressed in two small cell populations, most of which also express *Hoxa13* and *Hoxd13* (Figure 2A). At E13 and E15 stages, some *Dbx2*+ cells did not express *Hoxa13/Hoxd13* but displayed the *Col2a1* marker for mature cartilage precursors (Figure 2B, C). *Dbx2* transcripts were also detected in a subpopulation of *Hoxa13* and *Hoxd13* positive cells, which expressed the *Gdf5*, *Mlx*, *Scx*, and *Col1a1* genes as well (Figures 1C,D and 2B,C). *Gdf5* is transcribed in different cartilage and tendon-ligament precursors of the joint interzone, whereas *Mlx*, *Scx*, and *Col1a1* mark tendon cell precursors^{39–43} (Figure 1C,D). Of note, although *Dbx2/Col2a1/Sox9*+ cartilage cells did not express either *Hox13* genes at E13/E15, they derive from *Hox13*-positive cells (Figure 2A).³⁹

These results showed that *Dbx2* is expressed during digit development in *Hoxa13/Hoxd13* expressing cells corresponding to tendon and cartilage precursors of developing digit joints, thus supporting the possibility that HOX13 proteins could act as direct regulators of *Dbx2* expression in these cells, in agreement with the reported function of 5'*Hoxd* and *Hoxa13* genes in digit joint development.^{40,44,45}

2.2 | Identification of HOX13-bound sequences regulating *Dbx2* expression in digits

Dbx2 expression in distal limbs is strongly compromised in the absence of HOX13 proteins.²³ To further evaluate whether HOX13 paralogs could act as direct regulators of

Dbx2 expression, we set up to characterize the extent of the *Dbx2* regulatory landscape both by analyzing available Hi-C data sets and by performing 4C-seq experiments (Figures 3 and 4). TADs are megabase-scale structures that constitute a unit of 3D genome organization.^{37,50} Thus, they often coincide with and delimit the extent of gene regulatory landscapes.^{51,52} TADs are generally somewhat independent from the transcriptional status of the gene(s) inside and can be identified across different cell types or tissues.

We analyzed high-resolution (5 kb bin size) Hi-C data from ES cells and embryonic cortex,⁴⁶ as well as 40 kb-resolution Hi-C profiles from E12 mouse distal limbs⁴⁷ (Figure 3). We observed that, in all cases, the *Dbx2* genomic region is organized in two large TADs, which span the neighboring loci *Tmem117* and *Nell2* (5' TAD) and *Ano6*, *Arid2*, and *Scaf11* (3' TAD), respectively. Although with some variation between tissues or cell types, and depending on the TAD-separation score calculation parameters, the border between these two TADs consistently falls in the close vicinity of the *Dbx2* gene. Noteworthy, a region of ~150 kb spanning the *Dbx2* locus forms a micro-domain of higher contact frequency spanning the TAD boundary (hereafter referred to as inter-TAD domain) and the *Dbx2* interactions were mostly restricted to this interTAD domain. Accordingly, analysis of the binding profiles of CTCF (CCCTC-binding factor), a protein that plays an important role in the establishment of chromatin loops and TAD boundaries (e.g., references 53, 54) revealed that the *Dbx2* interTAD domain is flanked by two clusters of CTCF binding sites (BS) organized in large part in divergent orientations (Figure 3C). Besides, we observed a cluster of CTCF BSs located at the border of the *Nell2/Tmem117* interaction domain, in large part oriented convergently toward the CTCF sites lying at the 5' side of the *Dbx2* locus. While CTCF sites also delimit the *Ano6/Arid2* interaction

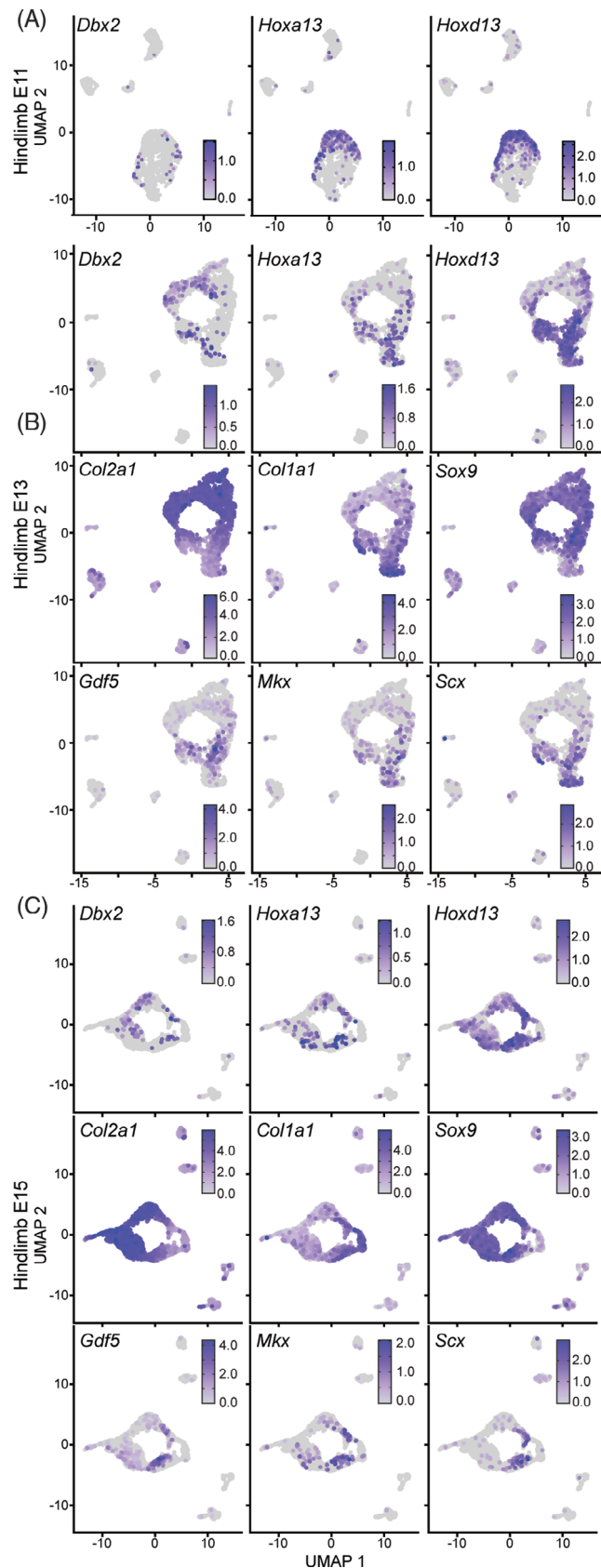


FIGURE 2 Single-cell RNAseq analysis of *Dbx2*+ cell populations in developing hindlimbs. UMAP representations of the scRNAseq data from mouse E11, A, E13, B, and E15, C, mouse hindlimbs³⁹ showing the expression of *Dbx2*, *Hoxa13*, and *Hoxd13*, as well as of different joint (*Gdf5*) and tendons/ligaments (*Mlx*, *Scx*) markers^{40–42}

domain, they are organized in the same orientation than those located on the 3' side of *Dbx2*, suggesting that both TADs flanking the *Dbx2* domain are established through different chromatin looping modalities.

To confirm this, we performed 4C-seq experiments by using mouse proximal and distal forelimb cells at E12 and the *Dbx2* promoter as a viewpoint (Figure 4A,B). As expected, the vast majority of *Dbx2* interactions were observed within the 150 kb region matching the inter-TAD domain identified in the Hi-C data analysis. However, some diffuse *Dbx2* interactions were also detected over the entire lengths of the 5' and 3' TADs flanking the *Dbx2* locus, whereas *Dbx2* contacts dramatically dropped down outside of these domains. Overall, the *Dbx2* interaction profiles remained very similar in both proximal and distal forelimbs (PFL and DFL, respectively). Nonetheless, we scored a DFL-specific increase in contacts over a narrow region located 55 kb away from the *Dbx2* transcription start site (TSS) on the 5' side of the locus, as well as with a broad region comprised between 82 and 236 kb 3' to the *Dbx2* transcription start site encompassing part of the neighboring *Ano6* gene (Figure 4C). These results suggested that *Dbx2* expression in the developing limbs is mostly driven by mid and short-range regulatory interactions within its immediate 150 kb surroundings.

To identify putative regulatory sequences controlling *Dbx2* expression in developing digits, we analyzed H3K27 acetylation data sets,²³ a histone modification specifically enriched in active enhancers and promoters.⁵⁵ In mouse E12 PFL and DFL cells, within the 800 kb spanned by *Dbx2* and its flanking TADs, we identified only five non-coding regions specifically enriched in H3K27ac (Figure 4B,C). These regions were located within the *Dbx2*-interTAD domain, suggesting that they could correspond to *Dbx2* regulatory elements. Of these, two were located in the intergenic region on the 5' side of the *Dbx2* locus, two others mapped within *Dbx2* intronic sequences whereas one overlapped with the first *Dbx2* exon and TSS. All these sequences were strongly contacted by the *Dbx2* promoter (Figure 4). Other H3K27ac-positive regions were identified within the *Ano6/Arid2/Scaf11* TAD, yet they were not specifically enriched in this epigenetic mark in DFL cells, arguing against a specific involvement of these sequences in *Dbx2* regulation.

We also analyzed HOXA13 and HOXD13 ChIP seq data sets²⁸ to determine whether these proteins would directly interact with the *Dbx2* locus (Figure 4B,C). We observed HOXA13/HOXD13 binding at several locations within the *Dbx2* genomic region. While most of these HOX13 bound sequences were not located in H3K27ac-positive and *Dbx2* interacting regions, we nevertheless observed strong binding of these proteins in three of the DFL-specific H3K27ac-positive sequences

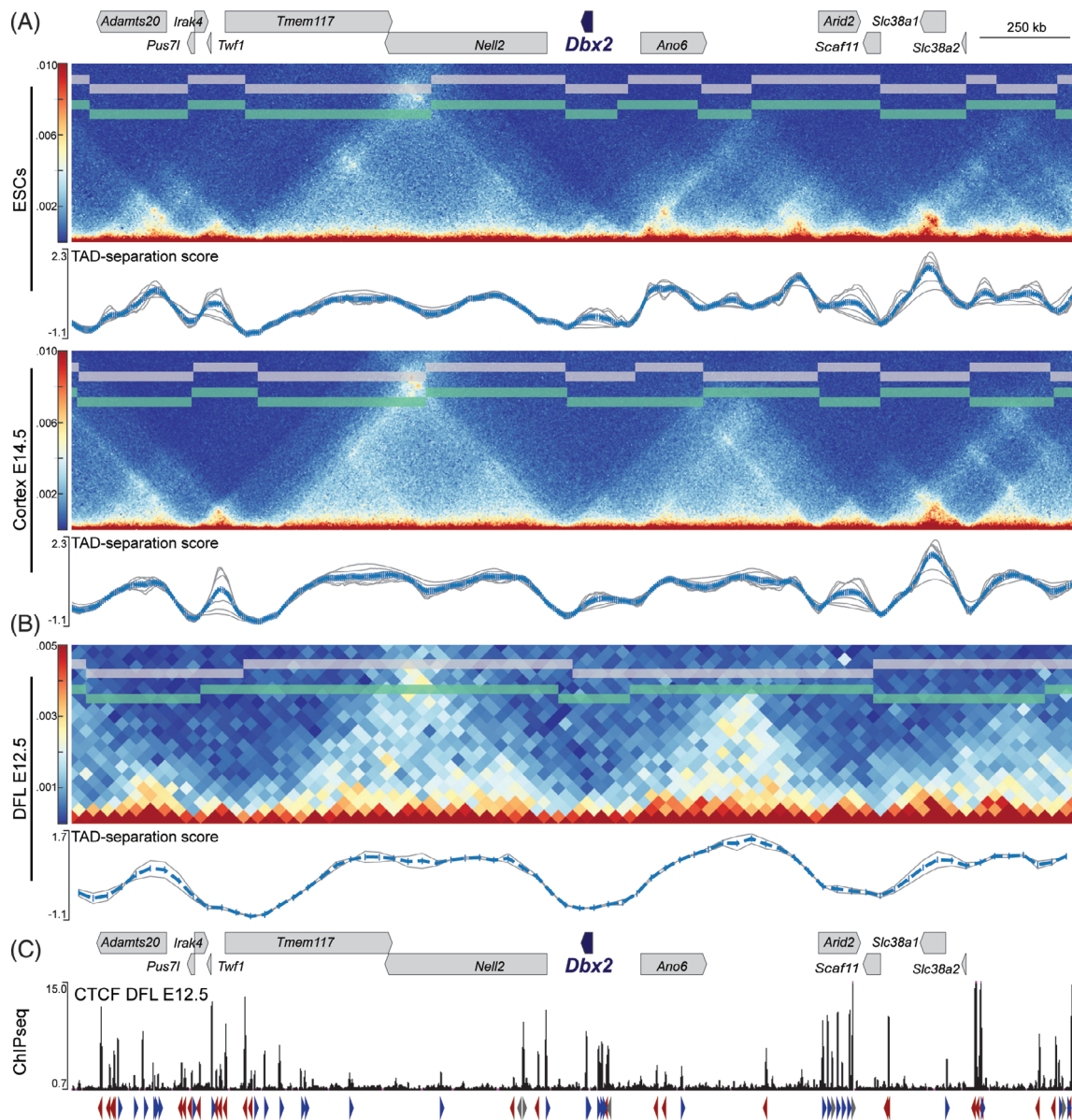


FIGURE 3 TAD organization around the *Dbx2* locus. A, High resolution (5 kb bin size) Hi-C map of the *Dbx2* genomic region in mouse ES cells (top) and E14 embryonic cortex (bottom), and graphs showing the TAD-separation score based on the HicFindTADs algorithm using different window size values (the curves calculated using standard parameters are displayed in gray and the average in blue). Data from Reference 46. B, 40 kb resolution (bin size) Hi-C map of the *Dbx2* genomic region in E12 mouse limb buds and graphs showing the TAD-separation score (as in A). Data from Reference 47. On top, the gene loci are represented in blue (*Dbx2*) or gray boxes for other genes. C, ChIPseq profile showing the CTCF binding coverage in the *Dbx2* genomic region in mouse E12 forelimbs.⁴⁸ Arrowheads below the CTCF peaks indicate BS orientation, determined using the CTCFBS prediction tool⁴⁹ (red: negative strand; blue: positive strand). Those BSs with a score < 5 or for which opposite orientations were predicted using different matrices are marked in gray. In the latter case, the orientation of the BS prediction with a higher score is indicated by the direction of the arrowhead

showing an interaction with *Dbx2*. One of these HOX13-bound sequences partially overlapped with a Vista enhancer (mm1571) previously characterized to drive *LacZ* reporter expression in the neural tube and developing limbs^{56,57} (Figure 5B, arrowhead). We quoted the other sequences as putative Distal Limb Enhancers (DLE) and numbered them based on their

5' to 3' position within the *Dbx2* interacting domain (DLE1 to DLE3). These sequences are largely conserved across mammals (Figure 5A). In addition, the Vista mm1571 enhancer is also conserved across tetrapods. Furthermore, we could identify evolutionarily conserved HOX13 BSs within the DLE1-3 Vista enhancer mm1571 sequences (Figure 5A).

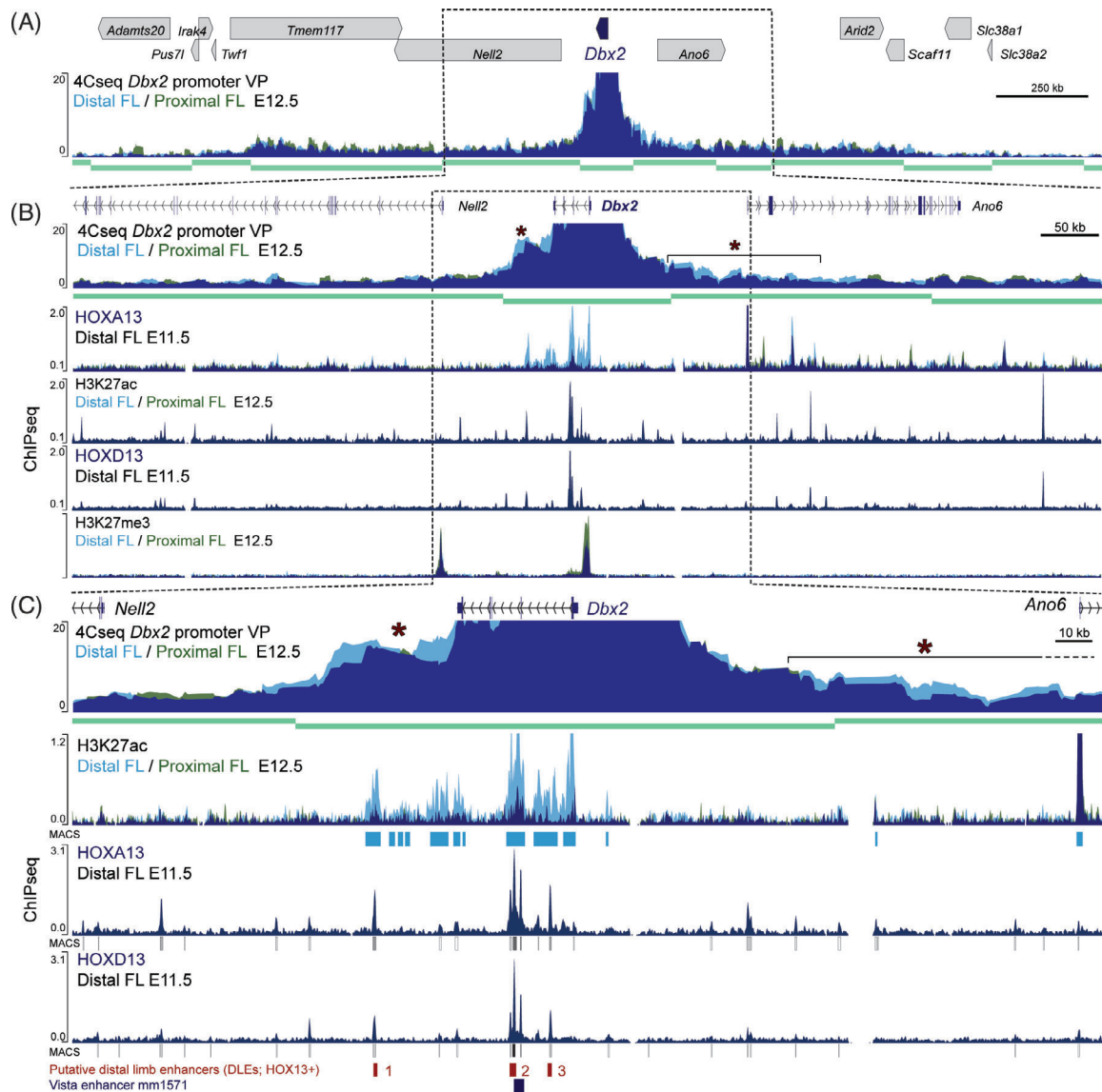


FIGURE 4 The *Dbx2* regulatory landscape in mouse limb buds. A, 4C-seq analysis of *Dbx2* interactions using the *Dbx2* promoter as a viewpoint in E12 mouse distal (light blue) and proximal (green) forelimbs. Profile overlap is in dark blue. Each curve marks the average profile of three independent biological replicates. Asterisks mark the region(s) displaying increased contact frequencies in the DFL vs. PFL. TADs in A and B are depicted with thick green lines. Protein coding loci are represented by blue (*Dbx2*) or gray boxes (all other genes) pointing toward the gene direction. B and C, 4C-seq and ChIP-seq analysis of H3K27ac and H3K27me3 marks in distal (light blue) and proximal (green) forelimbs, and HOXA13/HOXD13 binding profiles over the *Dbx2* genomic region (below) and their respective peak calling. Profile overlap is in dark blue. Data from References 23, 28. The HOX13 bound putative regulatory elements (DLE1 to 3) are shown in red. The region framed by a dashed line in B is displayed at a higher resolution in C. The Vista enhancer mm1571 is represented by a blue rectangle. Zoom in view of the 4C-seq and ChIP-seq profiles from B

To assess the functional role of these DLEs, we cloned the DLE1 and DLE2 sequences in a *LacZ* reporter vector and tested them in transient transgenic experiments. The two elements displayed activity in E13 DFLs in a domain reminiscent of *Dbx2* expression in the last forming joint of the phalanges (Figure 5B). Interestingly, DLE1 and DLE2 displayed mirror-imaged stainings, with DLE1 active in the posterior portion of the handplate and DLE2 anteriorly. Besides, DLE1 displayed a weak yet

reproducible activity in a narrow strip of cells within the mesopod (Figure 5B, asterisk), possibly related to the initial expression of *Dbx2* at E11.5 (Figure 1A, asterisk). This was maintained until E13, likely due to the stability of the beta-galactosidase protein. Neither DLE1 nor DLE2 displayed any transgene activity anywhere else than in developing digits. To corroborate the functional role of these elements on *Dbx2* regulation, we used CRISPR/Cas9 genome editing to produce mice lacking the DLE1

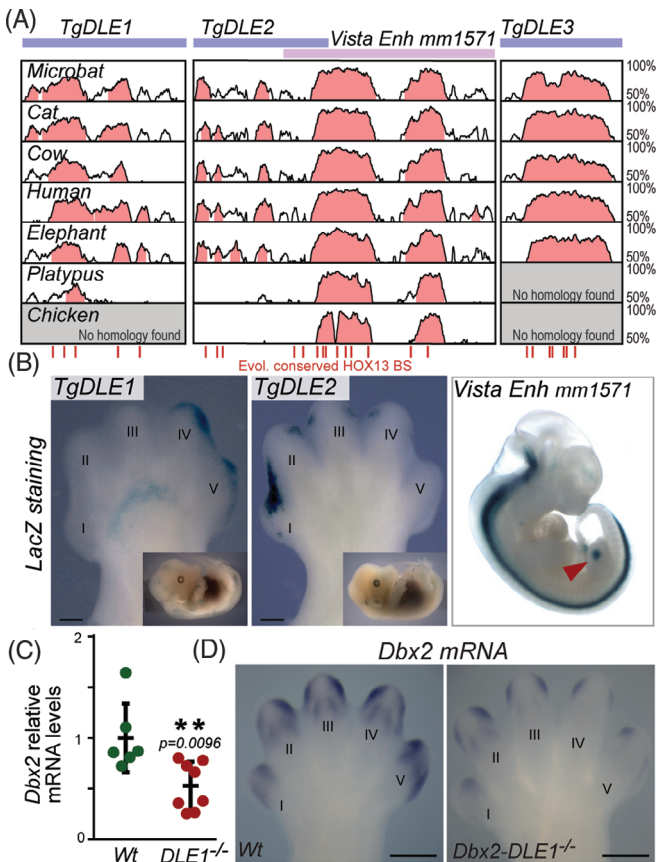


FIGURE 5 Putative *Dbx2* enhancers are active in distal limb buds. A, Vista alignment of the DLE1-3 regions and of the previously reported mm1571 regulatory element (depicted by purple and pink boxes, respectively). Evolutionarily conserved HOX binding sites are marked by vertical red lines at the bottom. B, X-gal staining of embryo transgenic for the DLE1 and DLE2 regulatory sequences in E13 mouse forelimbs (left) and of the mm1571 Vista enhancer (image from Vista enhancer browser; <https://enhancer.lbl.gov/>⁵⁷). Distal limb expression of the mm1571 enhancers is marked by a red arrowhead. C and D, Quantitative PCR, C, and WISH, D, analysis of *Dbx2* expression in the distal forelimb of wild-type (wt) and DLE1^{-/-} littermates. Each point represents independent biological replicates; bars represent the mean \pm SEM. Values are normalized to the *Hmbs* gene and to the wt. In B and D, Digits are numbered (I-V) in the anterior to posterior order. Scale bar: 250 μ m

regulatory element (DLE1^{-/-}). As expected, DLE1^{-/-} mice displayed a significant decrease in *Dbx2* expression in the E13 developing digits, as compared to control littermates (Figure 3C,D). In agreement with the DLE1 transgenesis results, this effect was even more pronounced in the posterior digits, where the DLE1 transgene displayed *LacZ* activity. Of note, *Dbx2* expression was also strongly affected in the joints of E13 DLE1^{-/-} embryos, despite the fact that the DLE1 transgene was not active in these regions, suggesting that a failure of DLE1-dependent *Dbx2* activation may have either

impaired or delayed its transcription at later phases of joint development. Alternatively, DLE1 activity in formed joints may require the synergistic cooperation of other elements to elicit a transcriptional response.

2.3 | *Hoxa13* and 5' *Hoxd* genes directly regulate *Dbx2* expression

To assess the relative contribution of *Hox13* paralogs to *Dbx2* regulation, we measured *Dbx2* expression in the forelimb autopods of either *Hoxa13*^{-/-} and *Hoxd13*^{-/-} mice, or of compound mutants carrying different combinations of *Hoxa13* and *Hoxd13* null alleles (Figure 6A), by using both WISH and qPCR. As previously described, *Dbx2* was almost completely abrogated in double *Hox13* mutant mice (Figure 6B,C). Instead, only a weak reduction in *Dbx2* expression was observed in *Hoxd13*^{-/-} single mutants. There, transcripts were maintained in the distal forelimb, with the exception of the posterior-most portion of the autopod, where *Dbx2* expression was severely reduced (Figure 6B,C). In contrast, *Dbx2* mRNA levels strongly decreased in *Hoxa13*^{-/-} embryos and transcripts remained detectable at low levels, in the distal portion of the central digits only. *Dbx2* expression was not scored neither in the *Hoxa13*^{-/-}*Hoxd13*^{+/-}, nor in the *Hoxa13*^{+/-}*Hoxd13*^{-/-} compound mutants (Figure 6B), indicating that a single allele of either genes was not sufficient to activate *Dbx2* in the DFL, despite the fact that in these mutants, a reduced but correctly specified autopod is still observed.^{17,23} Noteworthy, a faint and spatially ill-defined *Dbx2* signal was scored in the *Hox13* double knock-out mice (Figure 6B), reminiscent of the early expression of *Dbx2* in the incipient limb bud at E9.5 to E10 (Figure 1A). This expression was not observed in either *Hoxa13*^{-/-}*Hoxd13*^{+/-} or *Hoxa13*^{+/-}*Hoxd13*^{-/-} mutant embryos and may thus reflect the inability of *Hox13* mutant limbs to properly terminate the early limb developmental program and to initiate the transcriptional network operating at later stages in the autopodial domain.^{23,28}

Because *Hoxd* genes exert largely overlapping functions in the development of the distal limb domain,⁵⁸ we also assessed whether other *Hoxd* paralogs could contribute to *Dbx2* regulation. We analyzed *Dbx2* expression in series of mutant mice carrying deletions of different combinations of *Hoxd* genes (Figure 6A,D). *Hoxd*^{Del} (*Hoxd9-Hoxd12*) knock-out mice, hereafter referred to as Del (9-12), carry a deletion including all *Hoxd* genes normally expressed in the autopod but *Hoxd13*. They displayed normal levels of *Dbx2* expression as compared either to control or to *Hoxd13*^{-/-} mutant autopods. Instead, mice carrying a homozygote deletion including from *Hoxd8* to

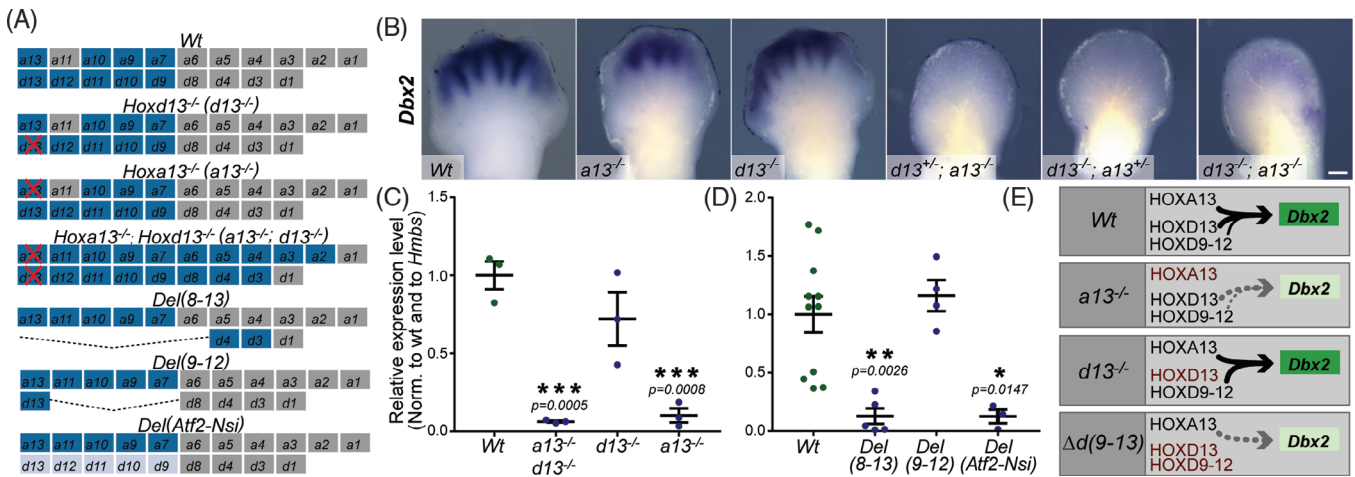


FIGURE 6 HOXA13 and 5' HOXD proteins cooperatively regulate *Dbx2* expression in developing digits. A, Scheme of the different *Hoxa* and *Hoxd* paralogs expressed (in blue) in wt distal limbs and in those of mice carrying homozygote mutations disrupting or altering the expression of the mouse *Hoxa13* and *Hoxd* paralogs. Silent genes are in gray. Red crosses represent inactivated genes. Dashed lines represent various deletions at the *HoxD* locus. The *Del(Atf2-Nsi)* mice carry a large genomic deletion spanning the centromeric TAD flanking *HoxD*. They display virtually no expression of any *Hoxd* genes in digits. B, WISH analysis of *Dbx2* expression in E12 mouse forelimbs of control and compound *Hoxa13/Hoxd13* mutant mice. Scale bar: 250 μ m. C and D, Quantitative PCR analysis of *Dbx2* expression in the DFL of control embryos or in different *Hoxa13*, *Hoxd13*, and *HoxD* mutant alleles. Each point represents independent biological replicates; bars represent the mean replicate value \pm SEM. P-values are calculated based on *t*-test comparison against wt values. E, Model explaining the cooperative role of *Hoxa13* and *Hoxd* genes in *Dbx2* regulation. Inactivated *Hoxa/Hoxd* paralogs in each mutant configuration are indicated in red. Arrow thickness represents the relative contribution of each HOX protein. Gray dashed arrows depict weak *Dbx2* activation

Hoxd13 (*HoxD^{Del(Hoxd8-Hoxd13)}-/-*; hereafter *Del(8-13)*) displayed a drastic downregulation of *Dbx2* mRNA levels, which was significantly stronger than that observed in *Hoxd13^{-/-}* mutant and comparable to that of *Hoxa13^{-/-}* mice. This reduction was also observed in mice carrying a large genomic deletion removing the *HoxD* centromeric gene desert, which contains all the elements controlling *Hoxd* gene expression in the autopod.⁵⁹ Altogether, these data indicate that although *Hoxd13* is the main *Hoxd* gene regulating *Dbx2* expression in digits, other *Hoxd* genes cooperatively contribute to this activation along with *Hoxa13* (Figure 6E).

2.4 | *Dbx2* does not significantly contribute to the distal limb skeleton development

To determine the extent to which *Dbx2* contributes to HOX13 functions in distal limbs, and also to assess its importance in the hand/foot phenotype associated with the deletion of the human *NELL2/DBX2/ANO6* genomic region,³⁶ we used CRISPR/Cas9 genome editing to disrupt the *Dbx2* homeodomain (Figure 7A). We designed specific sgRNAs targeting the flanking region of the *Dbx2* third exon, which encodes two out of the three alpha-helices (H1-H2) of the homeodomain and part of the

third (H3). We thus produced mice carrying a 377 bp large deletion, which removes the H1-2 coding sequence and produces a frameshift mutation disrupting also the third alpha-helix and the DBX2 C-terminal domain. This mutation is expected to prevent the binding of the protein to DNA and hence to inactivate its function (Figure 7A, B). The frequency of mouse pups carrying this *Dbx2* mutant allele, either heterozygous or homozygous, was significantly reduced when compared to the expected Mendelian ratio (Figure 7C), suggesting that the *Dbx2* mutation led to embryonic or perinatal lethality. However, no clear skeletal or hand/foot phenotype was observed in *Dbx2^{-/-}* mice, neither in the length or number of phalanges, nor in their degree of ossification or in their phalangeal joints (Figure 7D, F). Therefore, although *Dbx2* operates downstream of HOX13 genes in distal limb development, it is not the main contributor to the effects observed in these structures upon the loss of *Hox13* and other *Hoxd* genes.^{17,40,45}

2.5 | *Nell2/Dbx2/Ano6* coregulation in developing limbs

The absence of limb alterations in *Dbx2* null mice raised the question of whether the neighboring *Nell2* and *Ano6* genes may contribute to limb development. In fact, the

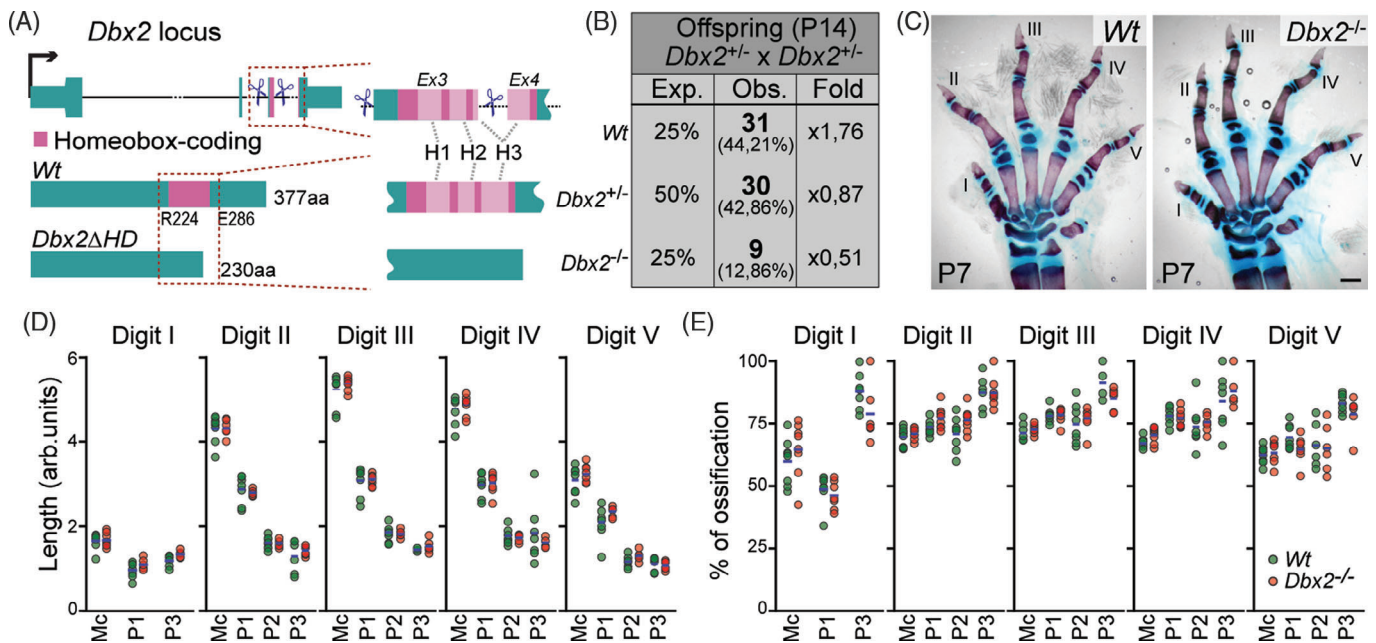


FIGURE 7 Disruption of the DBX2 homeodomain. A, *Dbx2* locus structure and predicted proteins in both control and mutated *Dbx2* alleles. Blue scissors indicate the sgRNAs used for CRISPR/Cas9 genome editing. The homeodomain-coding moiety is highlighted in pink. The first and last amino-acid positions of the DBX2 homeodomain are indicated. Its three α -helices (H1-3) are depicted by light pink boxes. Gray lines represent the correspondence between the DBX2 H1-H3 and its encoding sequence at the *Dbx2* locus. B, Table showing the proportion of *Dbx2*^{+/+}, *Dbx2*^{+/-}, and *Dbx2*^{-/-} P14 offspring obtained from *Dbx2*^{+/-} X *Dbx2*^{+/-} crosses. C, Alcian blue and alizarin red staining of the forelimb of P7 wt or *Dbx2*^{-/-} littermates. Digits are numbered (I-V) in the anterior to posterior order. Scale bar: 500 μ m. D and E, Quantification of the length, D, and degree of ossification, E, of metacarpals (Mc) and phalanges (P1-P3) of digits I to V in wt (green) or *Dbx2*^{-/-} (red) littermates. Bone length was calculated as the distance between the tips of the epiphysis. The degree of ossification was calculated as the ratio of the length of the alizarin red + domain and the total bone length. Each point represents a biological replicate. Blue lines depict the mean of all biological replicates

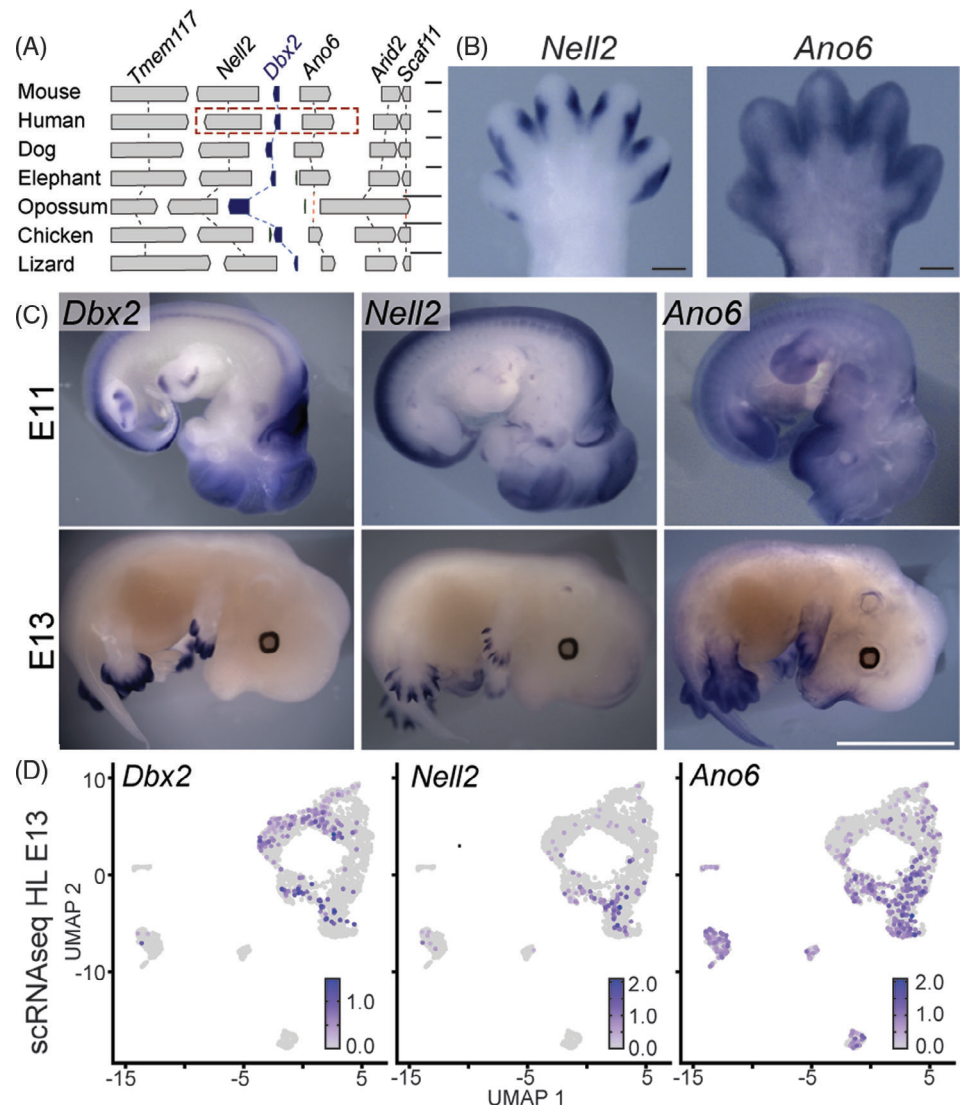
entire *Dbx2* genomic region has a syntenic interval in humans and other tetrapods (Figure 8A) and the deletion involved in hand-foot defects in humans also contains the *NELL2* and *ANO6* genes.³⁶ WISH analysis as well as mining a scRNA-seq data set³⁹ revealed that *Nell2* and *Ano6* are specifically expressed in the distal portion of mouse developing limbs, in a population of *Hoxa13/Hoxd13* double-positive cells, part of which also express *Dbx2* (Figure 8B-D). In both cases, their transcripts were distributed on both sides of the developing digits, displaying an indentation (*Nell2*) or a faint band (*Ano6*) corresponding to the joints of the forming phalanges (Figure 8B,C). However, we could not identify any DFL-specific H3K27ac positive region in the *Nell2* or *Ano6* TADs (Figure 4B,C), suggesting that their expression in developing limbs could be driven by the regulatory elements of the *Dbx2*-containing interTAD region.

To address this question, we performed 4C-seq experiment in E12 DFLs using either the *Nell2* or the *Ano6* promoters, as well as DLE1 and DLE2 as viewpoints (Figure 9A,B). As expected, the *Nell2* and *Ano6* promoters displayed strong interactions with sequences located in their own TADs, while they showed reduced

contacts with the neighboring TAD. However, in both cases, we observed significant contacts between both the *Nell2* and *Ano6* promoters and the DLE1-3 region (Figure 9A,B). In the reverse experiment, DLE1 interacted not only with the *Dbx2* promoter, but also with the close neighborhood of the *Nell2* and *Ano6* TSSs. Such interactions were also scored when using DLE2 as a viewpoint, although with a reduced intensity likely due to the fact that the DLE2 contacts remained overall strongly confined to the *Dbx2* interTAD domain. Nonetheless, DLE2 contacts with *Nell2/Ano6* were still higher than those displayed by the *Dbx2* promoter, which contacted predominantly the interTAD region (Figures 4 and 9A,B). We did not observe any significant enrichment of H3K27me3, a histone modification usually associated with inactive enhancers and promoters,⁶⁰ over the DLE1 to 3 regions (Figure 4B,C), ruling out the possibility that these interactions would represent contacts between H3K27me3 islands, as reported in other instances.⁶¹

To further document that part of the transcription of both *Nell2* and *Ano6* could be driven by elements shared with the *Dbx2*, we analyzed their expression in mice lacking the DLE1 sequence by WISH and qPCR. We

FIGURE 8 *Nell2* and *Ano6* expression in mouse limb buds. A, Synteny of the *Dbx2* genomic region. *Dbx2* is in blue and other genes in gray boxes. The red dashed rectangle depicts the deleted region reported in a human case.³⁶ Gray and red dashed lines indicate syntenic relationship and orthologous gene loss, respectively. Gene insertions are in green. Scale bar: 100 kb. B and C, WISH of *Dbx2*, *Nell2*, and *Ano6* in E13 mouse forelimbs, B, or in E11 to E13 whole embryos, C. D, UMAP representation of the scRNA-seq data from E13 mouse hindlimbs³⁹ for *Dbx2*, *Nell2* and *Ano6*



observed that *Nell2* and *Ano6* transcript levels were significantly decreased in the autopods of *DLE1*^{-/-} embryos when compared to control littermates (Figure 9C,D). This decrease was more pronounced for *Nell2* than for *Ano6*, yet it remained proportionally lower than that observed for *Dbx2* (Figure 5C,D), in agreement with the differences observed in contact frequency between DLE1-2 and the promoters of these three genes. These results supported the hypothesis that the regulatory elements located in the genomic vicinities of *Dbx2* also control part of the *Nell2* and *Ano6* expression in developing digits.

2.6 | Structural differences at the *Nell2/Dbx2/Ano6* locus between birds and eutherian mammals

While the DLE1 to 3 regulatory elements are broadly conserved across eutherians, they could not be identified

in nonmammalian tetrapods and we only observed a weak conservation for DLE1 in prototheria (opossum) (Figure 5A). Instead, a large syntenic region around the *Dbx2* locus is conserved across all tetrapods, except in monotremes where the *Ano6* gene was specifically lost (Figure 8A). Hi-C interaction profiles produced from embryonic chicken limbs⁶² revealed that the TAD organization of the chicken *Dbx2* region is similar to that of the mouse (Figures 3 and 10A), with *Dbx2* located in the close vicinity of the boundary between the *Nell2* and *Ano6* containing TADs (Figure 10A), in agreement with the syntenic correspondence. Accordingly, the distribution and orientation of CTCF sites in the chicken *Dbx2* genomic region are equivalent to those of the mouse, although with some differences (Figure 10A, bottom). The chicken *Dbx2* locus is also flanked by clusters of divergent CTCF sites, and the *Nell2*-containing TAD is delimited on its 5' side by CTCF sites oriented convergently toward those on the 5' side of *Dbx2*. Besides,

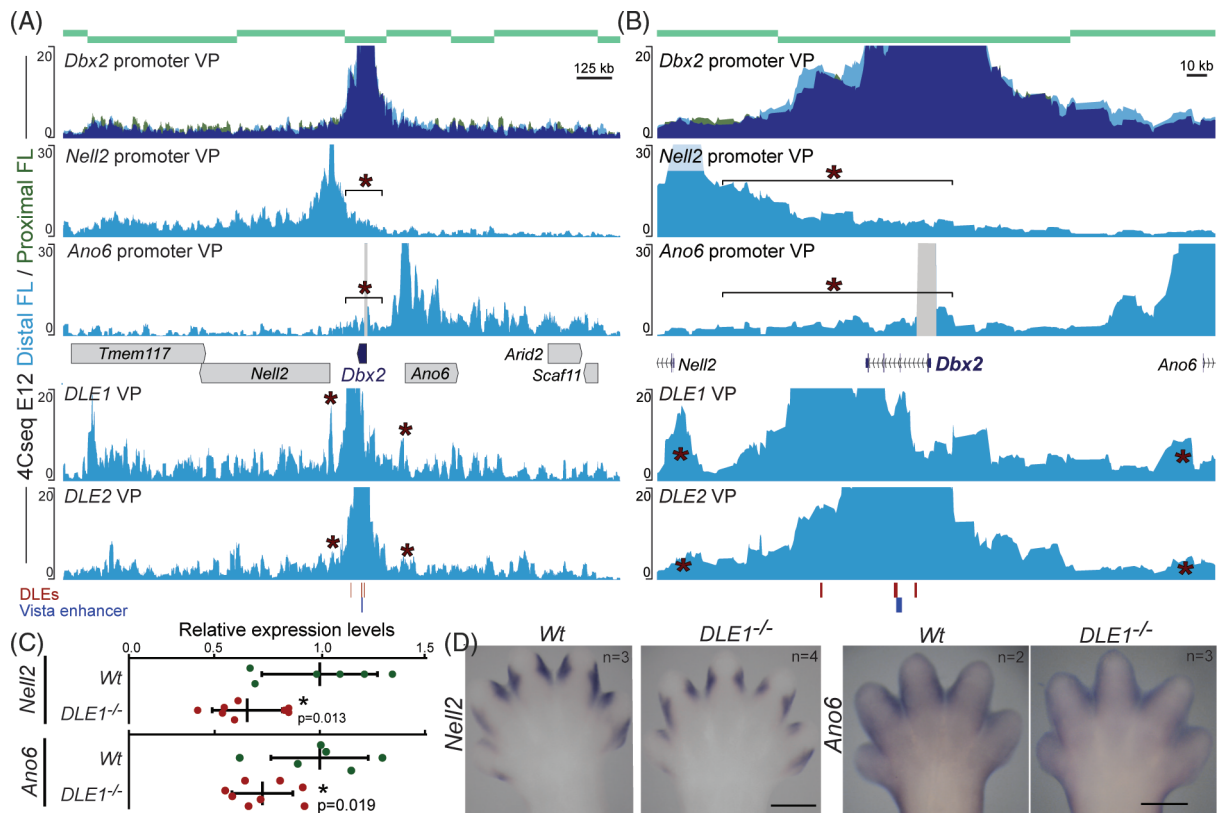


FIGURE 9 *Dbx2*, *Nell2*, and *Ano6* coregulation in mouse limb buds. A, 4C-seq profiles showing the interactions of *Dbx2*, *Nell2*, *Ano6*, DLE1, and DLE2 in proximal (green) and/or distal (light blue) forelimbs (profile overlap is in dark blue). The gray contacts in the *Ano6* viewpoint correspond to probably artefactual PCR product. *Nell2*, *Ano6*, DLE1, and DLE2 profiles are from a single experiment. The dashed rectangle represents the region analyzed in the right panel. C and D, Quantitative PCR, C, and WISH analysis, D, of *Nell2* and *Ano6* expression in E13 DFL of control and *DLE1*^{-/-} embryos. Each point represents independent biological replicates; bars represent the mean ± SEM. Values are normalized to the *Hmbs* gene and to the wt. Scale bar in B and F: 250 μm

the chicken *Ano6*/*Arid2* interacting domain is marked by CTCF sites organized in the same orientation but, unlike its mouse ortholog, the *Ano6*/*Arid2* intergenic region bears a high density of CTCF sites, indicating that this regulatory landscape evolved differently in the mouse and chicken lineages. This suggests that the *Dbx2* TAD architecture is maintained across tetrapods and arised before the emergence of mammals. We thus asked whether *Dbx2*, *Nell2*, and *Ano6* were expressed in the developing wings of chick embryos.

We did not observe any expression of either *Dbx2*, *Nell2*, or *Ano6* in the distal domain of embryonic chick limb buds (Figure 10B) by WISH. Although weak expression levels of *Dbx2*, *Ano6*, and *Nell2* transcripts were detected in RNAseq data, they were not specifically increased in the chicken autopod,⁶² in agreement with the idea that digit-specific expression of these genes was acquired after the emergence of the eutherian lineage. Instead, *Dbx2* was expressed in the developing chicken neural tube (Figure 10B), as expected from its expression

in the mouse CNS as well as by the activity of the evolutionary conserved mm1571 regulatory element in the neural tube (Figure 5A,B). Likewise, *Nell2* was expressed in the neural tube and somites of both species, in agreement with the function of this gene in sensory and motor neuron differentiation.^{63,64} *Ano6* transcripts were also detected in the paraxial and lateral mesoderm of both species. Therefore, *Dbx2*, *Nell2*, and *Ano6* expression in embryonic structures others than the developing digits is common to different tetrapod lineages, yet it is associated with different populations of neural and mesodermal precursors, suggesting that their transcription in these structures likely relies on gene-specific regulatory elements (Figures 8C and 10B). These results suggest an evolutionary scenario whereby the acquisition of distal limb enhancers within an ancestral TAD organization led to the co-option of *Nell2*, *Dbx2*, and *Ano6*, in the developing mouse digits (Figure 11). The functional consequences of this co-option remain to be established.

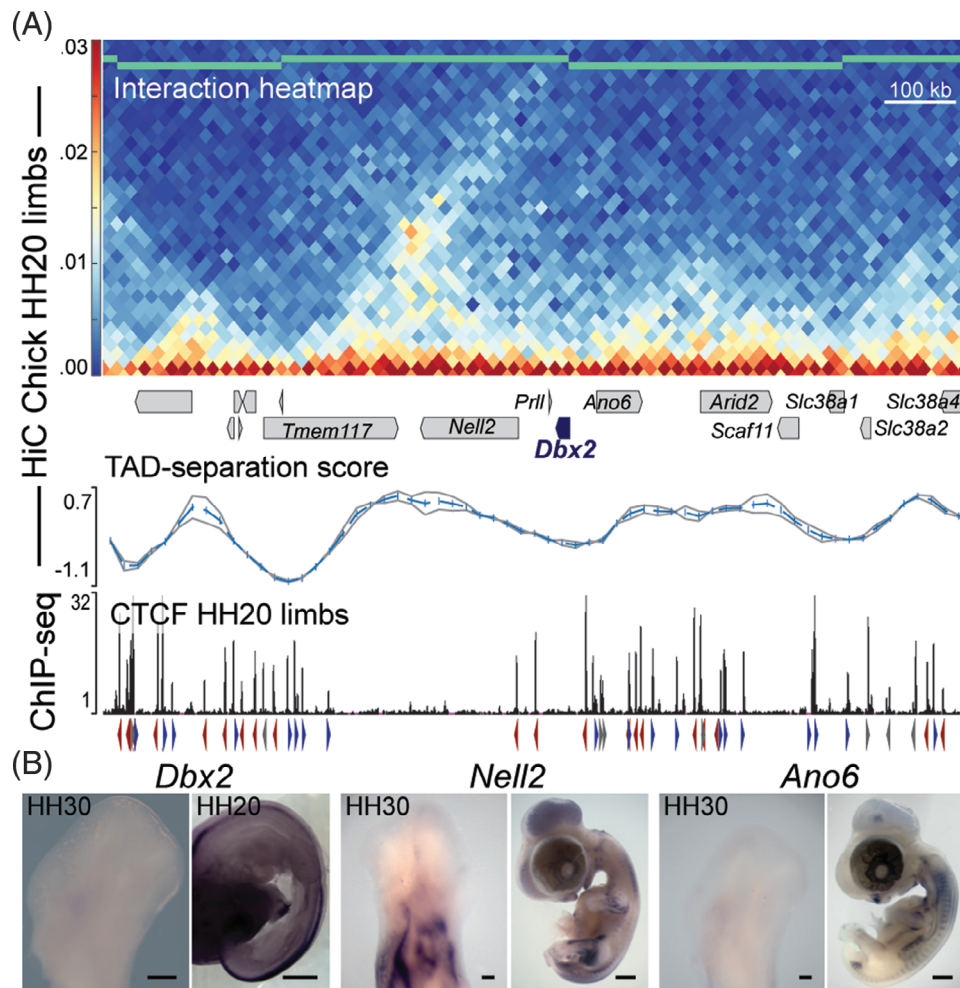


FIGURE 10 TAD structure and expression of the chicken *Nell2/Dbx2/Ano6* genes. A, Top, Hi-C map of the *Dbx2* genomic region in chicken HH20 wing buds and graphs showing the TAD-separation score (bottom) using standard window size parameters (gray lines; average in blue). Protein-coding gene loci are represented by blue (*Dbx2*) or gray boxes for all other genes. Data from Reference 62. TADs called by hicFindTADs are depicted with black boxes. Bottom, ChIPseq profile showing the CTCF binding coverage in the *Dbx2* genomic region in chicken HH20 limbs.⁶² Arrowheads below the CTCF peaks indicate the orientation of binding sites as determined by using the CTCFBS prediction tool⁴⁹ (red: negative strand; blue: positive strand). Those binding sites with a score < 5 or for which opposite orientations were predicted using different matrices are marked in gray. In the latter case, the orientation of the BS prediction with a higher score is indicated by the direction of the arrowhead. B, WISH analysis of *Dbx2*, *Nell2*, and *Ano6* expression in chicken wings and in HH20/HH30 embryos. Scale bar 250 μ m (limbs)/ 2 mm (embryos)

3 | DISCUSSION

3.1 | HOX13 mediated activation of *Dbx2* in digits and its function in distal limb development

In this study, we show that *Hoxa13* and posterior *Hoxd* genes directly activate *Dbx2* expression by binding to different regulatory elements located either within the *Dbx2* introns or in the 30 kb 5' to *Dbx2*. This is supported by the expression of these former genes in the autopod anlage, which precedes that of *Dbx2* by \sim 24 hours. Because HOX13 proteins have been proposed to act as

pioneer factors²⁵ (see also References 65), their binding at the *Dbx2* locus may facilitate the access to other transcription factors, thus explaining why some *Dbx2* expressing cells do not express any *Hox13* genes in E13 and E15 distal limbs whereas mice lacking all *Hox13* functions completely lose *Dbx2* expression. Besides binding to the DLE1 to DLE3 sequences, HOXA13 and HOXD13 also bind to various locations within the *Nell2/Dbx2/Ano6* genomic region. Many such sequences are only partially conserved across the eutherian lineage, in contrast with the high conservation of the DLE regions. While the functional significance of this large HOX13 coverage has not been addressed, it is clearly reminiscent

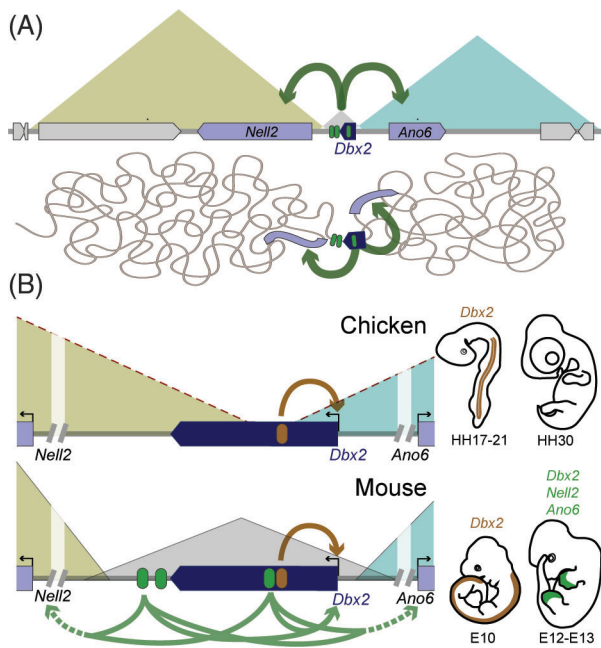


FIGURE 11 *Dbx2* regulation in mouse and chicken. A, Scheme of the TAD architecture of the mouse *Dbx2* genomic region (top) and its 3D organization (bottom). The *Dbx2* and *Nell2/Ano6* loci are depicted by blue and light purple boxes, respectively. All other genes are in gray boxes. DLE1 to 3 elements are shown in green. Green arrows indicate the regulation of DLE1 to 3 over *Nell2* and *Ano6* genes. B, Schemes of the TAD organization of the mouse and chicken *Dbx2* genomic region and its regulation. DLE1 to 3 and Vista mm1571 (or its chicken orthologous) elements are depicted by green and brown round boxes, respectively. Because of the low resolution of the chicken Hi-C, it was not possible to precisely resolve the location and extension of the *Dbx2* interTAD domain (approximate TADs limits are depicted by red dashed lines). Green and brown arrows point to the DLE1 to 3 and neural tube enhancer regulatory activity, respectively. No expression of *Dbx2*, *Nell2*, or *Ano6* was scored in the distal limb/wing of the chick embryo. In the mouse, the DLE1 to 3 sequences regulate the expression of *Dbx2*, *Nell2*, and *Ano6* in the developing distal limb

of that described for the TAD flanking the *HoxD* cluster, suggesting that HOX13 proteins may globally regulate the TAD activities at the *Dbx2* locus.²³

Mice lacking *Dbx2* function did not show any major skeletal anomaly, neither in the number of phalanges, their length or their ossification pattern, nor in their joints. Also, we did not observe any major limb alterations in the offspring of mice carrying a deletion of the DLE1 sequence, thus suggesting that *Dbx2* is likely not a major mediator of HOX13 function during distal development. The observed embryonic/perinatal lethality of *Dbx2*^{-/-} mice could result from defects in the specification of neuronal type in the CNS. However, *Dbx2*^{-/-} mice could display as yet undetected anomalies in the development and/or function of digital tendons and/or

ligaments, as suggested by the expression of this gene in precursors identified by the presence of transcripts from *Scx*, a known marker of tendon and ligament progenitor differentiation.^{42,66} Therefore, our results do not support the possibility that the loss of function of *DBX2* alone leads to the hand/foot defects observed in humans carrying a heterozygote deletion of the *NELL2/DBX2/ANO6* genomic region.³⁶ However, the observation that these genes are expressed during embryonic limb development indicates that their combined loss may generate these severe limb alterations. Accordingly, *Ano6* inactivation in mice was reported to affect bone formation and to result in micromelia.⁶⁷ Alternatively, the existence of a human-specific function of the *DBX2/NELL2/ANO6* genes in hand/foot development cannot be completely ruled out.

3.2 | Chromatin architecture and enhancer activity during *Nell2*, *Dbx2*, and *Ano6* coregulation

We used a comprehensive set of scRNA-seq, ChIP-seq, and Hi-C data to identify regulatory elements controlling *Dbx2* expression in digits and two such elements (DLE1 and 2) displayed enhancer activity in transgenic mice. The deletion of DLE1 leads to a strong down-regulation of *Dbx2* transcripts. The DLE1 to 3 sequences are evolutionarily conserved across eutherians, while they were not identified in non-mammalian tetrapods. Together with our observation that *Dbx2* is not expressed in embryonic chicken extremities, these observations suggest that limb-specific *Dbx2* expression evolved in the mammalian lineage. Also, the comparison of Hi-C interaction profiles at the *Dbx2* loci between mouse and chick revealed a similar TAD organization (Figure 11), which likely originated early in the tetrapod lineage, although we cannot exclude that more subtle changes in TAD architecture also contributed to the evolution of *Nell2/Dbx2* and *Ano6* expression in digits. In this context, the different distributions of CTCF binding sites in the mouse and chicken *Ano6* containing TADs may reflect this evolutionary divergence. However, while in chick the *Dbx2*, *Nell2*, and *Ano6* promoters are regulated mostly by locus-specific short or mid-range regulatory interactions, the mouse DLEs can co-regulate these three genes despite their location in different TADs.

This regulatory organization is reminiscent of that observed at the *HoxD* cluster, yet with an inversion of functionalities. At the *HoxD* locus, two flanking TADs contain distinct enhancers, which act in an exclusive manner upon *Hoxd* genes located at the TAD boundary (e.g., 65–67). At the *Dbx2* locus, the regulatory elements are located at the TAD boundary and can interact with

target genes located within the two adjacent TADs (Figure 11A), thus providing an original example of such a regulatory architecture. However, the functional contribution of this organization, as well as the mechanisms whereby the DLE sequences can differentially interact with the *Nell2/Dbx2* and *Ano6* promoters, remain to be determined. Recent reports have used chromosome engineering to analyze the insulating effect of TAD boundary regions,⁷¹⁻⁷³ supporting the conclusion that TADs are domains where enhancer-promoter contacts are favored, if not constrained. Our results suggest that, in some cases, enhancers located in between TADs may be selected to interact with either TAD depending on the context. Accordingly, it was recently shown that boundary elements can play an important role in allowing the establishment of interTAD promoter-enhancer interactions in drosophila embryos,⁷⁴ yet with a mechanism substantially different from the one proposed here. Another non-exclusive possibility is that *Dbx2* would be expressed in developing digits as a bystander effect due to the activity of the neighboring limb enhancers.⁷⁵

4 | EXPERIMENTAL PROCEDURES

4.1 | Mouse strains and transgenesis essays

Mice were kept and handled following good laboratory practices. Mutant strains were maintained in heterozygosis. The *Hoxd13*, *Hoxa13*, Del (1–13), De (8–13), and Del (9–12) mutant mouse lines (Figure 4) were previously described.^{17,20,76-78}

To generate the *Dbx2*^{+/-} and *DLE1*^{+/-} mutant lines, pairs of specific sgRNA targeting both sides of the *Dbx2* third exon (CTGCTGTTGAAAGTAGGACT; CCACTGTTCTGAGAGTCCGA) and the *DLE1* enhancer (GAAAA GGAAGACCACCCGTG; AGGGGCTAGAGATCTCC CAG) were co-electroporated together with the Cas9 protein (TruecutV2; Thermofisher), in fertilized mouse oocytes. To screen for each mutant allele, we designed specific primer pair flanking the *Dbx2* third exon and enhancer (*DLE1_F*: ACACACAGATAAATGCACGT GAAGTG; *DLE1_R*: GGAGGGCCACTCTTAGGTGTG). In each case, we selected F0 mouse mutant carrying a deletion of 377 bp (chr15: 95632232-95 632 608, mm10) spanning the whole *Dbx2* third exon, and a 1015 bp deletion (chr15:95600674-95 602 176, mm10) encompassing the *DLE1* sequence. Mutant mice were backcrossed with wt B6CBAF1 mice. Mutant F1 and F2 mice were selected using specific genotyping primers for their respective wt and mutated alleles (*Dbx2_F*: GGAAGTCCACCTT CGACTGACTG/ ACTGTTGATTAGGGCTGGGCTTTGA;

wt alleles: 756/ mutant allele 388 bp; *DLE1_wt*: GGAGTGAGGTTGTGCCAAGA/ ACCTGTAAGCCAAC CCCTAC; *DLE1_Mut*: ACACACAGATAAATGCACG TGA/ GAGGGCCACTCTTAGGGTGG).

For the transgenesis essays, the Tg*DLE1::LacZ* and Tg*DLE2::LacZ* plasmids were digested with NotI and KpnI. The fragment encoding the enhancer, b-globin minimal promoter and LacZ reporter was gel purified and injected in the masculine pronucleus of fertilized oocytes. Transgene injections were performed by the transgenesis platform of the University of Geneva. F0 embryos were dissected at E12-E13 and stained for LacZ activity.

4.2 | Probe, transgene, and sgRNA cloning

The sgRNA targeting guides were generated by annealing complementary pairs of oligonucleotides and cloned into the pX330 vector as described in.⁶⁹ The plasmid encoding the mouse *Dbx2* RNA probe was a gift from Thomas Jessell (Addgene plasmid 16288³³). Instead, specific primers were used to amplify a portion of the transcribed region of the mouse *Nell2*, *Ano6*, *Gdf5*, and *Mkx* genes as well as of the chicken *Dbx2*, *Nell2*, and *Ano6* orthologs. In each case, the PCR products were cloned into the pGEM-Teasy plasmid and sanger sequenced. For the chicken *Dbx2*, *Nell2* and *Ano6* genes, primers were designed based on the exon/intron structure predicted from the UCSC Non-Chicken Refseq genes, spliced EST, Chicken mRNA and Ensembl gene prediction.

For the transgenesis assays, the *DLE1/DLE2* sequences were amplified with specific primers (*DLE1* Fw: ATCCTGCTGTCTCTGGCTTTCAT/ GGGATCTGA TGCATGTAGTGGAAATTC; *DLE2* Fw: TCCAAGTTCTG TCTTCTAGGGCA/ GGATTGTGTATTAACCAGGACC GA) and cloned into the pSK-bglob::LacZ reporter plasmid,²³ generating the Tg*DLE1::LacZ* and Tg*DLE2::LacZ* reporter vectors.

4.3 | Probe and sgRNA preparation

For the sgRNA transcription, we PCR amplified the sgRNA sequence cloned into the pX330 plasmid using a T7 promoter containing primer and a universal reverse oligonucleotide (TAATACGACTCACTATAG). PCR products were gel purified and transcribed in vitro using the HiScribe T7 High Yield RNA Synthesis Kit (NEB). The transcribed sgRNAs were purified using the RNeasyTM mini kit (Qiagen). Gene-specific probes were synthesized in vitro by linearizing the respective coding

plasmids using specific restriction enzymes and by in vitro transcribed with either T7/T3 or Sp6 RNA polymerase. The probes were purified using the RNA easy mini kit.

4.4 | Gene expression analysis

For the qPCR analysis, pairs of E10/E11/E12/E13 mouse DFLs, as well as HH30-31 chicken distal wings, were microdissected and stored in RNAlater. Total RNA was extracted from each pair of DFLs/ distal wings using the Qiagen microRNA extraction kit and retro-transcribed using the Promega GOScript reaction mix with random primers. Gene expression levels were measured by real-time qPCR using the SYBR Select Master Mix for CFX (ThermoFisher), and specific primer pairs for the mouse *Dbx2*, *Hoxa13*, *Hoxd13* genes as well as for the chicken orthologs *Hoxd13* and *Dbx2* (Table 1). The mouse *Hmbs* and chicken *Gapdh* housekeeping genes were used as internal controls for the normalization of gene expression levels ($2^{-\Delta\Delta Ct}$). WISH experiments were performed as described in Reference 79.

4.5 | Skeletal preparation

Alcian blue and alizarin staining was performed as described in 56. Briefly, P7 mouse pups cadavers were eviscerated and skin and fat tissues were removed as much as possible. After 48 hours fixation in ethanol, cadavers were stained alcian blue solution (150 mg/L alcian blue 8 GX in 80% ethanol and 20% acetic acid) for 2 days and washed in 100% ethanol overnight. Subsequently, they were cleared for at least 3 hours in 2% KOH solution and stained for 2 hours in 50 mg/L alizarin red /

2% KOH solution. Finally, they were washed in 2% and 1% KOH solution and progressively dehydrated to 100% glycerol solution.

4.6 | Hi-C/ChIP seq/scRNA-seq data analysis, 4C-seq interaction profiling

All scripts used to analyze data and generate figures are available at <https://github.com/lldelisle/scriptsForBeccariEtAl2021>. The calculations were performed using the facilities of the Scientific IT and Application Support Center of EPFL. For the chicken Hi-C analysis, the raw forelimb and hindlimb data were extracted from GEO (see Table 2) and processed independently using HiCUP v0.8.0⁸⁰ on galGal6. Valid pairs were obtained using a custom python script. Both valid pair files were merged before analysis. Valid pairs from Hi-C carried out on mouse material were downloaded from GEO (see Table 2). Valid pairs of each study were loaded in a cool file using cooler version 0.8.10⁸¹ using a resolution of 5, 20, or 40 kb. The TAD-separation score and the domains were obtained using hicFindTADs version 3.5.2⁸²⁻⁸⁴ with `—minBoundaryDistance 100 000` and either default parameters for the choice of window size or a fixed window size of 120 kb. Plots were obtained using pyGenomeTracks version 3.6.^{82,85}

ChIP-seq paired-end (PE) fastq of HOXA13 and HOXD13 data, as well as single-read (SR) fastq from H3K27me3 and H3K27ac and corresponding inputs were downloaded from GEO (see Table 2). Adapter sequences and bad quality bases were removed with Cutadapt⁸⁶ version 1.16 with options `-a GATCGGAAGAGCACACGTCTGAACTCCAGTCAC -A GATCGGAAGAGCGTCGTGTAGGGAAAGAGTGTAGATCTCGGTGGTCGCCGTATCATT -q 30 -m 15` (`-A` being used only in PE data sets).

TABLE 1 Primers used for the cloning of RNA probes for in situ hybridization and for qPCR experiments

		Forward primer	Reverse primer
ISH probe	Mouse <i>Nell2</i>	GCGAAAACCCACAGTTGAC	TTCTTATCCAGGGGCGAGGAT
	Mouse <i>Ano6</i>	TCCCAGGCTCCTCGCAGCC	ACACGTGCGCACGGAGAGC
	Mouse <i>Gdf5</i>	GGCTCCCTGGTCTTCTTCAGCAGGA	GGTTTTCTTGCCAAGCCAGAG
	Mouse <i>Mkx</i>	CCAGCAGTGCTTGGGAAAAC	CAGTGAAGAGCTGTGCCTCAAACC
	Chick <i>Dbx2</i>	GTCTGCCATGAATTTTGCCCTC	GTGGTTTCAGTTTCACCCACAG
	Chick <i>Nell2</i>	GCATCTGGTCAAGTGTGGACTC	GTGGATCCACAGTGCCTTCAG
	Chick <i>Ano6</i>	CACGTACATATACTTTGTGAAG	CAAGAATTACTTGTGTGAAG
qPCR analysis	Mouse <i>Dbx2</i>	AGGTGCCTCCAAGAAGGTCTT	GTGGTTTCAGTTTCACCCACAGGA
	Mouse <i>Nell2</i>	AATGGAACCACGTGCAAAGC	ACACATTGGCAGCAATGCAC
	Mouse <i>Ano6</i>	TGCCTTGCTCGCTGAAAAAG	TGGCAAGCAGAGAAGTCAGTAG
	Mouse <i>Hmbs</i>	CGGCTTCTGCAGACACCAG	CCCTCATCTTTGAGCCGTTTT

Reads were mapped with bowtie 2.3.5⁸⁷ with default parameters on mm10. Alignments with a mapping quality below 30 were discarded with samtools view version 1.9.^{88,89} For HOXA13 and HOXD13, coverage and peak calling were computed by macs2 version 2.1.1.20160309 with options

—call-summits -f BAMPE -B. Coverage was then normalized by the number of million fragments used in macs2 coverage. For histone marks, coverage and peak calling were computed by macs2 with options -f BAM—nomodel—extsize 200—broad using the BAM of input in -c. The coverage was then normalized by the number of million tags used in macs2 coverage. Plots were obtained using pyGenomeTracks version 3.6.^{82,85} For DFL_E12_H3K27ac, the two replicates were averaged.

TABLE 2 GEO data sets used in this study

	GEO accession number	Reference
HiC mouse E14 Cortex, ES cells	GSE96107, GSE161259	46
HiC mouse DFLs	GSE101715	47
HiC chicken HH20 FLs and HLs	GSM3182470, GSM3182471	62
HOXA13 and HOXD13 binding in DFLs	GSE81358	28
H3K27ac and H3K27me3 coverage in DFLs and PFLs	GSE77900	23
CTCF binding in mouse E12 DFLs	GSM2535578	48
CTCF binding in CHICKEN HH20 FLs	GSM3182452	62

For the scRNA-seq, matrices with counts were downloaded from GEO (see Table 2). UMAP and expression plots were obtained using Seurat package version 3.2.2⁹⁰ on each data set individually.

We performed our 4C-seq experiments according to.⁹¹ Briefly, 12 pairs of wild-type DFLs or PFLs were dissected, dissociated with collagenase (Sigma Aldrich/Fluka) and filtered through a 35 µm mesh to isolate single cells. Cells were fixed with 2% formaldehyde (in PBS/10%FBS) for 10 minutes at room temperature and the reaction was quenched on ice with glycine. Cells were further lysed with 10 mM Tris pH 7.5, 10 mM NaCl, 5 mM MgCl₂, 0.1 mM EDTA, 1x Protease inhibitor cocktail to isolate nuclei and stored at -80°C. Nuclei from pools of at least 10 distal or proximal limbs were digested with DpnII (New England Biolabs) and ligated with T4

TABLE 3 4Cseq primers

Viewpoint	Primer (Fw and Rv)
<i>Dbx2 promoter</i>	A34_Fw: AATGATACGGCGACCACCGAACACTCTTTCCCTACACGACGCTCTTCCGATCT ACAT AGCTAAATGTCCTTCTTTGGGGGATC G24_Fw: AATGATACGGCGACCACCGAACACTCTTTCCCTACACGACGCTCTTCCGATCT GGTA AGCTAAATGTCCTTCTTTGGGGGATC C14_Fw: AATGATACGGCGACCACCGAACACTCTTTCCCTACACGACGCTCTTCCGATCT CAGA AGCTAAATGTCCTTCTTTGGGGGATC T34_Fw: AATGATACGGCGACCACCGAACACTCTTTCCCTACACGACGCTCTTCCGATCT TTAG AGCTAAATGTCCTTCTTTGGGGGATC Rv: CAAGCAGAAGACGGCATAACGAAAAGACGTCCTTTGTAGGCATG
<i>DLE1</i>	T14_Fw: AATGATACGGCGACCACCGAACACTCTTTCCCTACACGACGCTCTTCCGATCT TGAC AGACTGGAACGCGTAGTTTCTGATC Rv: CAAGCAGAAGACGGCATAACGACACAACCTCACTCCTTTCTTGTAC
<i>DLE2</i>	A34_Fw: AATGATACGGCGACCACCGAACACTCTTTCCCTACACGACGCTCTTCCGATCT ACAT GGGCATTAGTTTGTGCTGGGTAAATTCAG Rv: CAAGCAGAAGACGGCATAACGACACAAGTTTCCCTTTCATTTAGCTGG
<i>Nell2 promoter</i>	T14_Fw: AATGATACGGCGACCACCGAACACTCTTTCCCTACACGACGCTCTTCCGATCT TGAC CGCCCATCAACTTGGCACCTG Rv: CAAGCAGAAGACGGCATAACGAAAGCCCACTCACTGTTGACCATAC
<i>Ano6 promoter</i>	A34_Fw: AATGATACGGCGACCACCGAACACTCTTTCCCTACACGACGCTCTTCCGATCT ACAT TCCCAGGCTCCTCGCAGCC Rv: CAAGCAGAAGACGGCATAACGAAACACGTCGCGACGGAGAGC

Note: The sequences corresponding to the Illumina adaptors and barcodes are marked in blue and in red, respectively.

DNA ligase HC (Promega) in diluted conditions to promote intramolecular ligation. Samples were digested again with NlaIII (New England Biolabs) and ligated with T4 DNA ligase HC (Promega) in diluted conditions. These templates were amplified using Expand long template (Roche) and inversed PCR primers flanked with adaptors allowing multiplexing (Table 3). Barcodes (4 bp) were added between the Illumina adaptor and the specific DpnII primers. Libraries were prepared by means of 8-10 independent PCR reactions using 70 to 100 ng of DNA per reaction. PCR products were pooled and purified using the PCR purification kit (Qiagen). Multiplexed libraries were sequenced on Illumina HiSeq 2500 at the Sequencug platform of the University of Geneva to obtain 100 bp single-end reads. Demultiplexing, mapping and 4C-seq analysis were performed using a local version of the pipeline described in,⁹² on the mouse assembly GRCm38 (mm10). The profiles were smoothed using a window size of 11 fragments and normalized to the mean score in ± 5 Mb around the viewpoint. When multiple independent biological replicates were available, average 4C-seq profiles were calculated.

4.7 | Data availability

Data are available in GEO (accession number: GSE161386).

4.8 | Phylogenetic footprinting and HOX13/CTCF binding site analysis

The genomic sequence of the mouse DLE1 to 3 and Vista enhancer 1571 were used to identify their orthologous sequences in other mammalian and tetrapods species using the NCBI BLAST alignment tool⁹³ with sensitive parameters. Orthologous sequences were then aligned using the Vista alignment tools^{94,95} (Shuffle-LAGAN algorithm). Evolutionary conserved binding sites for HOX13 proteins were identified with the ConTra v3 tool (<http://bioit2.irc.ugent.be>),⁹⁶ using the Transfac⁹⁷ HOXA13 position weight matrixes and stringent parameters (core = 0.95, similarity matrix = 0.85). A predicted HOX13 BS was considered evolutionary conserved when it could be identified in at least four of the six mammalian species used in the multispecies alignment (human, cat, cow, elephant, rabbit, and opossum). For the identification of the CTCF binding sites in the mouse and chicken *Dbx2* genomic regions, as well as the analysis of their orientation, we used the CTCFBS Prediction Tool (<http://insulatordb.uthsc.edu/>).⁴⁹

ACKNOWLEDGMENTS

We thank the transgenesis and sequencing platforms of the University of Geneva. We also thank Aurélie Hintermann for help in chick embryo dissections and for discussions.

AUTHOR CONTRIBUTIONS

Leonardo Beccari: Conceptualization; formal analysis; investigation; methodology; project administration; supervision; writing-original draft; writing-review & editing. **Gabriel Jaquier:** Investigation; methodology. **Lucille Lopez-Delisle:** Data curation; formal analysis; methodology; software; validation; writing-review & editing. **Eddie Rodriguez-Carballo:** Investigation; methodology; resources. **Benedicte Mascrez:** Investigation; resources. **Sandra Gitto:** Formal analysis; resources.

CONFLICT OF INTEREST

The authors declare no competing interests.

ORCID

Leonardo Beccari  <https://orcid.org/0000-0001-6472-5105>

Denis Duboule  <https://orcid.org/0000-0001-9961-2960>

REFERENCES

1. Saunders JW Jr, Gasseling MT. Ectodermal-mesenchymal interactions in the origins of limb symmetry. In: Fleischmajer R, Billingham RE, eds. *Epithelial-Mesenchymal Interactions*. Baltimore, Maryland: Williams and Wilkins; 1968:78-97.
2. Tickle C, Shellswell G, Crawley A, Wolpert L. Positional signaling by mouse limb polarising region in the chick wing bud. *Nature*. 1976;259(5542):396-397. <https://doi.org/10.1038/259396a0>.
3. Fallon JF, Saunders JW. In vitro analysis of the control of cell death in a zone of prospective necrosis from the chick wing bud. *Dev Biol*. 1968;18(6):553-570. [https://doi.org/10.1016/0012-1606\(68\)90026-2](https://doi.org/10.1016/0012-1606(68)90026-2).
4. Tabin C, Wolpert L. Rethinking the proximodistal axis of the vertebrate limb in the molecular era. *Genes Dev*. 2007;21(12):1433-1442. <https://doi.org/10.1101/gad.1547407>.
5. Wellik D, Sun X, Boekhoff-Falk G, John F, Fallon, PhD: fifty years of excellence in limb research and counting. *Dev Dyn*. 2011;240(5):909-914. <https://doi.org/10.1002/dvdy.22594>.
6. Dahn RD, Fallon JF. Interdigital regulation of digit identity and homeotic transformation by modulated BMP signaling. *Science*. 2000;289(5478):438-441. <https://doi.org/10.1126/science.289.5478.438>.
7. Rowe DA, Fallon JF. The proximodistal determination of skeletal parts in the developing chick leg. *J Embryol Exp Morphol*. 1982;68:1-7.
8. Fallon J, Lopez A, Ros M, Savage M, Olwin B, Simandl B. FGF-2: apical ectodermal ridge growth signal for chick limb development. *Science*. 1994;264(5155):104-107. <https://doi.org/10.1126/science.7908145>.
9. Maas SA, Fallon JF. Single base pair change in the long-range sonic hedgehog limb-specific enhancer is a genetic basis for

- preaxial polydactyly. *Dev Dyn*. 2005;232(2):345-348. <https://doi.org/10.1002/dvdy.20254>.
10. Dollé P, Izpisua-Belmonte J-C, Falkenstein H, Renucci A, Duboule D. Coordinate expression of the murine Hox-5 complex homeobox-containing genes during limb pattern formation. *Nature*. 1989;342(6251):767-772. <https://doi.org/10.1038/342767a0>.
 11. Lewis J, Martin P. Vertebrate development. Limbs: a pattern emerges. *Nature*. 1989;342(6251):734-735. <https://doi.org/10.1038/342734a0>.
 12. Laufer E, Nelson CE, Johnson RL, Morgan BA, Tabin C. Sonic hedgehog and Fgf-4 act through a signaling cascade and feedback loop to integrate growth and patterning of the developing limb bud. *Cell*. 1994;79(6):993-1003. [https://doi.org/10.1016/0092-8674\(94\)90030-2](https://doi.org/10.1016/0092-8674(94)90030-2).
 13. Lewandoski M, Sun X, Martin GR. Fgf8 signalling from the AER is essential for normal limb development. *Nat Genet*. 2000;26(4):460-463. <https://doi.org/10.1038/82609>.
 14. Niswander L, Tickle C, Vogel A, Booth I, Martin GR. FGF-4 replaces the apical ectodermal ridge and directs outgrowth and patterning of the limb. *Cell*. 1993;75(3):579-587.
 15. Haack H, Gruss P. The establishment of murine Hox-1 expression domains during patterning of the limb. *Dev Biol*. 1993;157(2):410-422. <https://doi.org/10.1006/dbio.1993.1145>.
 16. Davis AP, Witte DP, Hsieh-Li HM, Potter SS, Capecchi MR. Absence of radius and ulna in mice lacking hoxa-11 and hoxd-11. *Nature*. 1995;375(6534):791-795. <https://doi.org/10.1038/375791a0>.
 17. Fromental-Ramain C, Warot X, Messadecq N, LeMeur M, Dolle P, Chambon P. Hoxa-13 and Hoxd-13 play a crucial role in the patterning of the limb autopod. *Development*. 1996;122(10):2997-3011.
 18. Kmita M, Tarchini B, Zákány J, Logan M, Tabin CJ, Duboule D. Early developmental arrest of mammalian limbs lacking HoxA/HoxD gene function. *Nature*. 2005;435(7045):1113-1116. <https://doi.org/10.1038/nature03648>.
 19. Zakany J, Duboule D. The role of Hox genes during vertebrate limb development. *Curr Opin Genet Dev*. 2007;17(4):359-366. <https://doi.org/10.1016/j.gde.2007.05.011>.
 20. Dollé P, Dierich A, LeMeur M, et al. Disruption of the Hoxd-13 gene induces localized heterochrony leading to mice with neonatal limbs. *Cell*. 1993;75(3):431-441. [https://doi.org/10.1016/0092-8674\(93\)90378-4](https://doi.org/10.1016/0092-8674(93)90378-4).
 21. Yokouchi Y, Nakazato S, Yamamoto M, et al. Misexpression of Hoxa-13 induces cartilage homeotic transformation and changes cell adhesiveness in chick limb buds. *Genes Dev*. 1995;9(20):2509-2522. <https://doi.org/10.1101/gad.9.20.2509>.
 22. Zákány J, Fromental-Ramain C, Warot X, Duboule D. Regulation of number and size of digits by posterior Hox genes: a dose-dependent mechanism with potential evolutionary implications. *Proc Natl Acad Sci U S A*. 1997;94(25):13695-13700. <https://doi.org/10.1073/pnas.94.25.13695>.
 23. Beccari L, Yakushiji-Kaminatsui N, Woltering JM, et al. A role for HOX13 proteins in the regulatory switch between TADs at the HoxD locus. *Genes Dev*. 2016;30(10):1172-1186. <https://doi.org/10.1101/gad.281055.116>.
 24. Cobb J, Duboule D. Comparative analysis of genes downstream of the Hoxd cluster in developing digits and external genitalia. *Development*. 2005;132(13):3055-3067. <https://doi.org/10.1242/dev.01885>.
 25. Desanlis I, Kherdjemil Y, Mayran A, et al. HOX13-dependent chromatin accessibility underlies the transition towards the digit development program. *Nat Commun*. 2020;11(1):2491. <https://doi.org/10.1038/s41467-020-16317-2>.
 26. Knosp WM, Scott V, Bächinger HP, Stadler HS. HOXA13 regulates the expression of bone morphogenetic proteins 2 and 7 to control distal limb morphogenesis. *Development*. 2004;131(18):4581-4592. <https://doi.org/10.1242/dev.01327>.
 27. Salsi V, Zappavigna V. *Hoxd13* and *Hoxa13* directly control the expression of the *EphA7* Ephrin tyrosine kinase receptor in developing limbs. *J Biol Chem*. 2006;281(4):1992-1999. <https://doi.org/10.1074/jbc.M510900200>.
 28. Sheth R, Barozzi I, Langlais D, et al. Distal limb patterning requires modulation of cis-regulatory activities by HOX13. *Cell Rep*. 2016;17(11):2913-2926. <https://doi.org/10.1016/j.celrep.2016.11.039>.
 29. Yamamoto S, Uchida Y, Ohtani T, et al. Hoxa13 regulates expression of common Hox target genes involved in cartilage development to coordinate the expansion of the autopodal anlage. *Develop Growth Differ*. 2019;61(3):228-251. <https://doi.org/10.1111/dgd.12601>.
 30. Johnson KR, Lu S, Murtha MT, Ruddle FH, Davisson MT. Genetic mapping of a new homeobox gene to mouse chromosome 7. *Genomics*. 1992;14(4):1107-1109.
 31. Shoji H, Ito T, Wakamatsu Y, et al. Regionalized expression of the Dbx family homeo genes in the embryonic CNS of the mouse. *Mech Dev*. 1996;56(1):25-39. [https://doi.org/10.1016/0925-4773\(96\)00509-6](https://doi.org/10.1016/0925-4773(96)00509-6).
 32. Briscoe J, Pierani A, Jessell TM, Ericson J. A Homeodomain protein code specifies progenitor cell identity and neuronal fate in the ventral neural tube. *Cell*. 2000;101(4):435-445. [https://doi.org/10.1016/S0092-8674\(00\)80853-3](https://doi.org/10.1016/S0092-8674(00)80853-3).
 33. Pierani A, Brenner-Morton S, Chiang C, Jessell TM. A sonic hedgehog-independent, retinoid-activated pathway of neurogenesis in the ventral spinal cord. *Cell*. 1999;97(7):903-915. [https://doi.org/10.1016/S0092-8674\(00\)80802-8](https://doi.org/10.1016/S0092-8674(00)80802-8).
 34. Timmer JR, Wang C, Niswander L. BMP signaling patterns the dorsal and intermediate neural tube via regulation of homeobox and helix-loop-helix transcription factors. *Development*. 2002;129(10):2459-2472.
 35. Wijgerde M, McMahon JA, Rule M, McMahon AP. A direct requirement for hedgehog signaling for normal specification of all ventral progenitor domains in the presumptive mammalian spinal cord. *Genes Dev*. 2002;16(22):2849-2864. <https://doi.org/10.1101/gad.1025702>.
 36. Carlsen EØ, Frengen E, Fannemel M, Miscio D. Haploinsufficiency of ANO6, NELL2 and DBX2 in a boy with intellectual disability and growth delay. *Am J Med Genet A*. 2015;167(8):1890-1896. <https://doi.org/10.1002/ajmg.a.37079>.
 37. Dixon JR, Selvaraj S, Yue F, et al. Topological domains in mammalian genomes identified by analysis of chromatin interactions. *Nature*. 2012;485(7398):376-380. <https://doi.org/10.1038/nature11082>.
 38. Yokouchi Y, Sasaki H, Kuroiwa A. Homeobox gene expression correlated with the bifurcation process of limb cartilage development. *Nature*. 1991;353(6343):443-445. <https://doi.org/10.1038/353443a0>.
 39. Kelly NH, Huynh NPT, Guilak F. Single cell RNA-sequencing reveals cellular heterogeneity and trajectories of lineage

- specification during murine embryonic limb development. *Matrix Biol.* 2020;89:1-10. <https://doi.org/10.1016/j.matbio.2019.12.004>.
40. Huang B-L, Trofka A, Furusawa A, et al. An interdigit signaling Centre instructs coordinate phalanx-joint formation governed by 5'Hoxd-Gli3 antagonism. *Nat Commun.* 2016;7(1):12903. <https://doi.org/10.1038/ncomms12903>.
 41. Liu W, Watson SS, Lan Y, et al. The atypical Homeodomain transcription factor Mohawk controls tendon morphogenesis. *Mol Cell Biol.* 2010;30(20):4797-4807. <https://doi.org/10.1128/MCB.00207-10>.
 42. Shwartz Y, Viukov S, Krief S, Zelzer E. Joint development involves a continuous influx of Gdf5-positive cells. *Cell Rep.* 2016;15(12):2577-2587. <https://doi.org/10.1016/j.celrep.2016.05.055>.
 43. Murchison ND, Price BA, Conner DA, et al. Regulation of tendon differentiation by scleraxis distinguishes force-transmitting tendons from muscle-anchoring tendons. *Development.* 2007;134(14):2697-2708. <https://doi.org/10.1242/dev.001933>.
 44. Perez WD, Weller CR, Shou S, Stadler HS. Survival of Hoxa13 homozygous mutants reveals a novel role in digit patterning and appendicular skeletal development. *Dev Dyn.* 2010;239(2):446-457. <https://doi.org/10.1002/dvdy.22183>.
 45. Villavicencio-Lorini P, Kuss P, Friedrich J, et al. Homeobox genes d11-d13 and a13 control mouse autopod cortical bone and joint formation. *J Clin Invest.* 2010;120(6):1994-2004. <https://doi.org/10.1172/JCI41554>.
 46. Bonev B, Cohen NM, Szabo Q, et al. Multiscale 3D genome rewiring during mouse neural development. *Cell.* 2017;171(3):557-572.e24. <https://doi.org/10.1016/j.cell.2017.09.043>.
 47. Rodriguez-Carballo E, Lopez-Delisle L, Zhan Y, et al. The HoxD cluster is a dynamic and resilient TAD boundary controlling the segregation of antagonistic regulatory landscapes. *Genes Dev.* 2017;31(22):2264-2281. <https://doi.org/10.1101/gad.307769.117>.
 48. Fabre PJ, Leleu M, Mormann BH, et al. Large scale genomic reorganization of topological domains at the HoxD locus. *Genome Biol.* 2017;18(1):149. <https://doi.org/10.1186/s13059-017-1278-z>.
 49. Ziebarth JD, Bhattacharya A, Cui Y. CTCFBSDB 2.0: a database for CTCF-binding sites and genome organization. *Nucleic Acids Res.* 2013;41:D188-D194. <https://doi.org/10.1093/nar/gks1165>.
 50. Dixon JR, Gorkin DU, Ren B. Chromatin domains: the unit of chromosome organization. *Mol Cell.* 2016;62(5):668-680. <https://doi.org/10.1016/j.molcel.2016.05.018>.
 51. de Laat W, Duboule D. Topology of mammalian developmental enhancers and their regulatory landscapes. *Nature.* 2013;502(7472):499-506. <https://doi.org/10.1038/nature12753>.
 52. Symmons O, Uslu VV, Tsujimura T, et al. Functional and topological characteristics of mammalian regulatory domains. *Genome Res.* 2014;24(3):390-400. <https://doi.org/10.1101/gr.163519.113>.
 53. Phillips-Cremens JE, Sauria MEG, Sanyal A, et al. Architectural protein subclasses shape 3D Organization of Genomes during lineage commitment. *Cell.* 2013;153(6):1281-1295. <https://doi.org/10.1016/j.cell.2013.04.053>.
 54. Nora EP, Goloborodko A, Valton A-L, et al. Targeted degradation of CTCF decouples local insulation of chromosome domains from genomic compartmentalization. *Cell.* 2017;169(5):930-944.e22. <https://doi.org/10.1016/j.cell.2017.05.004>.
 55. Creighton MP, Cheng AW, Welstead GG, et al. Histone H3K27ac separates active from poised enhancers and predicts developmental state. *Proc Natl Acad Sci.* 2010;107(50):21931-21936. <https://doi.org/10.1073/pnas.1016071107>.
 56. Oosterveen T, Kurdija S, Alekseenko Z, et al. Mechanistic differences in the transcriptional interpretation of local and long-range Shh morphogen signaling. *Dev Cell.* 2012;23(5):1006-1019. <https://doi.org/10.1016/j.devcel.2012.09.015>.
 57. Visel A, Minovitsky S, Dubchak I, Pennacchio LA. VISTA enhancer browser—a database of tissue-specific human enhancers. *Nucleic Acids Res.* 2007;35(Database issue):D88-D92. <https://doi.org/10.1093/nar/gkl822>.
 58. Delpretti S, Zakany J, Duboule D. A function for all posterior Hoxd genes during digit development? *Dev Dyn.* 2012;241(4):792-802. <https://doi.org/10.1002/dvdy.23756>.
 59. Montavon T, Soshnikova N, Mascrez B, et al. A regulatory archipelago controls Hox genes transcription in digits. *Cell.* 2011;147(5):1132-1145. <https://doi.org/10.1016/j.cell.2011.10.023>.
 60. Bernstein BE, Mikkelsen TS, Xie X, et al. A bivalent chromatin structure marks key developmental genes in embryonic stem cells. *Cell.* 2006;125(2):315-326. <https://doi.org/10.1016/j.cell.2006.02.041>.
 61. Vieux-Rochas M, Fabre PJ, Leleu M, Duboule D, Noordermeer D. Clustering of mammalian Hox genes with other H3K27me3 targets within an active nuclear domain. *Proc Natl Acad Sci.* 2015;112(15):4672-4677. <https://doi.org/10.1073/pnas.1504783112>.
 62. Yakushiji-Kaminatsui N, Lopez-Delisle L, Bolt CC, Andrey G, Beccari L, Duboule D. Similarities and differences in the regulation of HoxD genes during chick and mouse limb development. *PLoS Biol.* 2018;16(11):e3000004. <https://doi.org/10.1371/journal.pbio.3000004>.
 63. Nelson BR, Matsushashi S, Lefcort F. Restricted neural epidermal growth factor-like like 2 (NELL2) expression during muscle and neuronal differentiation. *Mech Dev.* 2002;119:S11-S19. [https://doi.org/10.1016/S0925-4773\(03\)00084-4](https://doi.org/10.1016/S0925-4773(03)00084-4).
 64. Nelson BR, Claes K, Todd V, Chaverra M, Lefcort F. NELL2 promotes motor and sensory neuron differentiation and stimulates mitogenesis in DRG in vivo. *Dev Biol.* 2004;270(2):322-335. <https://doi.org/10.1016/j.ydbio.2004.03.004>.
 65. Amândio AR, Lopez-Delisle L, Bolt CC, Mascrez B, Duboule D. A complex regulatory landscape involved in the development of mammalian external genitals. *elife.* 2020;9:e52962. <https://doi.org/10.7554/eLife.52962>.
 66. Shukunami C, Takimoto A, Nishizaki Y, et al. Scleraxis is a transcriptional activator that regulates the expression of tenomodulin, a marker of mature tenocytes and ligamentocytes. *Sci Rep.* 2018;8(1):3155. <https://doi.org/10.1038/s41598-018-21194-3>.
 67. Ehlen HWA, Chinenkova M, Moser M, et al. Inactivation of anoctamin-6/Tmem16f, a regulator of phosphatidylerine scrambling in osteoblasts, leads to decreased mineral deposition in skeletal tissues. *J Bone Miner Res.* 2013;28(2):246-259. <https://doi.org/10.1002/jbmr.1751>.
 68. Andrey G, Montavon T, Mascrez B, et al. A switch between topological domains underlies HoxD genes collinearity in mouse limbs. *Science.* 2013;340(6137):1234167. <https://doi.org/10.1126/science.1234167>.
 69. Darbellay F, Bochaton C, Lopez-Delisle L, et al. The constrained architecture of mammalian Hox gene clusters. *Proc*

- Natl Acad Sci U S A.* 2019;116(27):13424-13433. <https://doi.org/10.1073/pnas.1904602116>.
70. Lonfat N, Montavon T, Darbellay F, Gitto S, Duboule D. Convergent evolution of complex regulatory landscapes and pleiotropy at Hox loci. *Science.* 2014;346(6212):1004-1006. <https://doi.org/10.1126/science.1257493>.
 71. Gómez-Marín C, Tena JJ, Acemel RD, et al. Evolutionary comparison reveals that diverging CTCF sites are signatures of ancestral topological associating domains borders. *Proc Natl Acad Sci USA.* 2015;112(24):7542-7547. <https://doi.org/10.1073/pnas.1505463112>.
 72. Ibn-Salem J, Köhler S, Love MI, et al. Deletions of chromosomal regulatory boundaries are associated with congenital disease. *Genome Biol.* 2014;15(9):423. <https://doi.org/10.1186/s13059-014-0423-1>.
 73. Lupiáñez DG, Kraft K, Heinrich V, et al. Disruptions of topological chromatin domains cause pathogenic rewiring of gene-enhancer interactions. *Cell.* 2015;161(5):1012-1025. <https://doi.org/10.1016/j.cell.2015.04.004>.
 74. Yokoshi M, Segawa K, Fukaya T. Visualizing the role of boundary elements in enhancer-promoter communication. *Mol Cell.* 2020;78(2):224-235.e5. <https://doi.org/10.1016/j.molcel.2020.02.007>.
 75. Cajiao I, Zhang A, Yoo EJ, Cooke NE, Liebhaber SA. Bystander gene activation by a locus control region. *EMBO J.* 2004;23(19):3854-3863. <https://doi.org/10.1038/sj.emboj.7600365>.
 76. Spitz F, Gonzalez F, Peichel C, Vogt TF, Duboule D, Zákány J. Large scale transgenic and cluster deletion analysis of the HoxD complex separate an ancestral regulatory module from evolutionary innovations. *Genes Dev.* 2001;15(17):2209-2214. <https://doi.org/10.1101/gad.205701>.
 77. Tarchini B, Duboule D. Control of Hoxd Genes' collinearity during early limb development. *Dev Cell.* 2006;10(1):93-103. <https://doi.org/10.1016/j.devcel.2005.11.014>.
 78. Tschopp P, Duboule D. A regulatory 'landscape effect' over the HoxD cluster. *Dev Biol.* 2011;351(2):288-296. <https://doi.org/10.1016/j.ydbio.2010.12.034>.
 79. Woltering JM, Noordermeer D, Leleu M, Duboule D. Conservation and divergence of regulatory strategies at Hox loci and the origin of tetrapod digits. *PLoS Biol.* 2014;12(1):e1001773. <https://doi.org/10.1371/journal.pbio.1001773>.
 80. Lieberman-Aiden E, van Berkum NL, Williams L, et al. Comprehensive mapping of long-range interactions reveals folding principles of the human genome. *Science.* 2009;326(5950):289-293. <https://doi.org/10.1126/science.1181369>.
 81. Abdennur N, Mirny LA. Cooler: scalable storage for hi-C data and other genomically labeled arrays. *Bioinformatics.* 2020;36(1):311-316. <https://doi.org/10.1093/bioinformatics/btz540>.
 82. Ramírez F, Bhardwaj V, Arrigoni L, et al. High-resolution TADs reveal DNA sequences underlying genome organization in flies. *Nat Commun.* 2018;9(1):189. <https://doi.org/10.1038/s41467-017-02525-w>.
 83. Wolff J, Bhardwaj V, Nothjunge S, et al. Galaxy HiCEXplorer: a web server for reproducible hi-C data analysis, quality control and visualization. *Nucleic Acids Res.* 2018;46(W1):W11-W16. <https://doi.org/10.1093/nar/gky504>.
 84. Wolff J, Rabbani L, Gilsbach R, et al. Galaxy HiCEXplorer 3: a web server for reproducible hi-C, capture hi-C and single-cell hi-C data analysis, quality control and visualization. *Nucleic Acids Res.* 2020;48(W1):W177-W184. <https://doi.org/10.1093/nar/gkaa220>.
 85. Lopez-Delisle L, Rabbani L, Wolff J, et al. pyGenomeTracks: reproducible plots for multivariate genomic data sets. *Bioinformatics.* 2020;btaa692. <https://doi.org/10.1093/bioinformatics/btaa692>.
 86. Martin M. Cutadapt removes adapter sequences from high-throughput sequencing reads. *EMBnet J.* 2011;17(1):10-12. <https://doi.org/10.14806/ej.17.1.200>.
 87. Langmead B, Salzberg SL. Fast gapped-read alignment with bowtie 2. *Nat Methods.* 2012;9(4):357-359. <https://doi.org/10.1038/nmeth.1923>.
 88. Li H. A statistical framework for SNP calling, mutation discovery, association mapping and population genetical parameter estimation from sequencing data. *Bioinformatics.* 2011;27(21):2987-2993. <https://doi.org/10.1093/bioinformatics/btr509>.
 89. Li H, Handsaker B, Wysoker A, et al. The sequence alignment/map format and SAMtools. *Bioinformatics.* 2009;25(16):2078-2079. <https://doi.org/10.1093/bioinformatics/btp352>.
 90. Stuart T, Butler A, Hoffman P, et al. Comprehensive integration of single-cell data. *Cell.* 2019;177(7):1888-1902.e21. <https://doi.org/10.1016/j.cell.2019.05.031>.
 91. Noordermeer D, Leleu M, Splinter E, Rougemont J, De Laat W, Duboule D. The dynamic architecture of Hox gene clusters. *Science.* 2011;334(6053):222-225. <https://doi.org/10.1126/science.1207194>.
 92. David FPA, Delafontaine J, Carat S, et al. HTSstation: a web application and open-access libraries for high-throughput sequencing data analysis. *PLoS One.* 2014;9(1):e85879. <https://doi.org/10.1371/journal.pone.0085879>.
 93. Madden TL, Tatusov RL, Zhang J. Applications of network BLAST server. *Methods Enzymol.* 1996;266:131-141. [https://doi.org/10.1016/s0076-6879\(96\)66011-x](https://doi.org/10.1016/s0076-6879(96)66011-x).
 94. Frazer KA, Pachter L, Poliakov A, Rubin EM, Dubchak I. VISTA: computational tools for comparative genomics. *Nucleic Acids Res.* 2004;32(suppl 2):W273-W279. <https://doi.org/10.1093/nar/gkh458>.
 95. Mayor C, Brudno M, Schwartz JR, et al. VISTA: visualizing global DNA sequence alignments of arbitrary length. *Bioinformatics.* 2000;16(11):1046-1047. <https://doi.org/10.1093/bioinformatics/16.11.1046>.
 96. Kreft L, Soete A, Hulpiau P, Botzki A, Saey Y, De Bleser P. ConTra v3: a tool to identify transcription factor binding sites across species, update 2017. *Nucleic Acids Res.* 2017;45(W1):W490-W494. <https://doi.org/10.1093/nar/gkx376>.
 97. Matys V, Kel-Margoulis OV, Fricke E, et al. TRANSFAC and its module TRANSCOMP: transcriptional gene regulation in eukaryotes. *Nucleic Acids Res.* 2006;34:D108-D110. <https://doi.org/10.1093/nar/gkj143>.

How to cite this article: Beccari L, Jaquier G, Lopez-Delisle L, et al. *Dbx2 regulation in limbs suggests interTAD sharing of enhancers. Developmental Dynamics.* 2021;250:1280-1299. <https://doi.org/10.1002/dvdy.303>